Evaluation of atmospheric aerosols in the Metropolitan Area of São Paulo simulated by the regional EURAD-IM model on high-resolution

Ediclê De Souza Fernandes Duarte[1], Philipp Franke[2,3], Anne Caroline Lange[2,3], Elmar Friese[2,3], Fábio Juliano da Silva Lopes[4,5], Jonatan João da Silva[5,6], Jean Souza dos Reis[1], Eduardo Landulfo[5], Cláudio Moises Santos e Silva[7], Hendrik Elbern[2], Judith Johanna Hoelzemann[7,*]

[1]*Graduate Program in Climate Sciences, Federal University of Rio Grande do Norte, Natal/RN, Brazil*

[2]*Rhenish Institute for Environmental Research at the University of Cologne, Köln, Germany*

[3]*Institute of Energy and Climate Research: Troposphere (IEK-8), Forschungszentrum Jülich GmbH, Jülich, Germany*

[4]*Environmental Science Department, Institute of Environmental, Chemical and Pharmaceutical Science, Federal University of São Paulo, Rua São Nicolau, 210, Centro, Diadema, São Paulo 09913-030, Brazil*

[5]*Centre for Laser and Applications, Nuclear and Energy Research Institute, São Paulo, Brazil*

[6]*Center for Exact Sciences and Technologies, Federal University of Western Bahia, Brazil*

[7]*Department of Atmospheric and Climate Sciences, Federal University of Rio Grande do Norte, Natal/RN, Brazil*

**Corresponding authors: JJH (judith.hoelzemann@ccet.ufrn.br)*

ABSTRACT

We present a high-resolution air quality study over São Paulo, Brazil with the EURopean Air Pollution Dispersion - Inverse Model (EURAD-IM) used for the first time over South America simulating detailed features of aerosols. Modeled data are evaluated with observational surface data and a Lidar. Two case studies in 2016 with distinct meteorological conditions and pollution plume features show transport (i) from central South America, associated to biomass burning activities, (ii) from the rural part of the state of São Paulo, (iii) between the metropolitan areas of Rio de Janeiro and São Paulo (MASP) either through the Paraíba Valley or via the ocean, connecting Brazil's two largest cities, (iv) from the port-city Santos to MASP and also from MASP to the city Campinas, and vice versa. A Pearson coefficient of 0.7 was found for PM10 at MASP CENTER and EURAD-IM simulations vary within the observational standard deviation, with a Mean Percentual Error (MPE) of 10 %. The model's vertical distributions of aerosol layers agree with the Lidar profiles that show either characteristics of long-range transported biomass burning plumes, or of local pollution. The distinct transport patterns that agree with satellite Aerosol Optical Death and fire spot images as well as with the ground-based observations within the standard deviations, allows us exploring patterns of air pollution in a detailed manner and to understand the complex interactions between local to long-range transport sources.

Keywords: Mesoscale modeling, Regional transport of aerosols, Model evaluation, Air pollution, Brazil, Urban areas.

INTRODUCTION

Global air pollution emissions have strongly increased due to transportation, energy production and industrial activities, mostly concentrated in densely populated areas. Such conditions give rise to numerous public health problems such as cardio-respiratory diseases and agents of premature deaths (Saldiva et al., 1994; Faiz et al., 1996; Lanki et al., 2006; Gurjar et al., 2008; Asmi et al. 2009). Environmental impacts are particularly severe in cities of about 10 million or more inhabitants - also known as megacities. According to United Nations (2018), in 2018, 1.7 billion people, which corresponds to 23 % of the world's population, lived in a city with at least 1 million inhabitants, while this number is projected to accrue to 28 % by 2030. These cities range from urban areas with relatively clean air in industrialized nations to highly polluted cities in the developing countries (Molina and Molina, 2002; Molina and Molina, 2004, Molina et al., 2007, Gulia et al., 2015). Thus, megacities tend to be global risk areas due to a dense concentration of people and extreme dynamics. Their inhabitants are vulnerable to air pollution inducing adverse health impacts (Gurjar et al., 2008). Such risks need to be estimated to support national and international efforts to improve the sustainability of megacity life worldwide.

Atmospheric models with explicit treatment of the physical and chemical processes have become powerful means to the studies of the urban air pollution impacts. A plethora of modeling studies is available focusing on different aspects of the pollution impact, such as pollution episodes (Jiang et al., 2017), regional and long-distance transport (Tie et al., 2007; Lin et al., 2010; Andrade et al., 2015; Rafee et al, 2017; Albuquerque et al., 2018), secondary formation of gases and particles (Jiang et al., 2012; Lowe et al., 2015; Wang et al., 2016; Vara-Vela et al., 2018), and the effects of land use and land cover changes (Capucim et al., 2015; Rafee et al., 2015).

In general, Chemistry Transport Models (CTMs) are tools that simulate the formation, transport, chemical transformation, and deposition of particles and gas-phase species. The level of sophistication depends on the degree of the model's complexity. By simulating the weather and air quality of a region it is possible to assess the current level of pollution (Alonso et al., 2010; Vara-Vela et al., 2016, 2018; Albuquerque et al., 2018; Pedruzzi et al., 2019), track trends (Carvalho et al., 2015; Andrade et al., 2015; Zhang et al., 2018), define responsibilities for air pollution levels (Ring et al., 2018; Song et al., 2019), assess the potential impact of future emission sources (Collet et al., 2018; Campbell et al., 2018), study emission reduction scenarios (Alonso et al., 2010; Andrade et al., 2012; Wang et al., 2016; Albuquerque et al., 2019; Yu et al., 2019; Andreão et. al., 2020, Pinto et al., 2020) and estimate the health impacts (Boldo et al., 2014; Ding et al., 2016; Andreão et al., 2018; Li et al., 2019, Andreão et al., 2020). Applications of regional air quality models across several parts of the world include for example WRF-Chem (Zhang et al., 2008; Andrade et al., 2015; Rafee et al., 2017; Bahreini et al., 2018), WRF-SMOKE-CMAQ (Albuquerque et al., 2018), BRAMS (Longo et al., 2010; Moreira et al., 2013;), POLAIR 3D (Wang et al., 2015); EURAD-IM (Ebel et al., 1997; Elbern et al., 2007 and 2010).

In Brazil, many studies have been made by using the Brazilian Regional Atmospheric Modeling System (BRAMS) applied with the purpose of forecasting not only the atmospheric behavior but also air quality (Pielke et al., 1992; Masson, 2000; Rozoff et al. 2003; Cotton et al., 2003; Freitas et al., 2005; Freitas

et al., 2007, 2007a, 2007b, 2009, 2017; Longo et al., 2010). Another model that is widely used in Brazil is the Weather Research and Forecast with Chemistry (WRF-Chem) model (Grell et al. 2005). The WRF-Chem model was employed for air quality forecasting in south-eastern Brazil (Andrade et al., 2015), studying how vehicular emissions can affect fine particle formation (Vara-Vela et al., 2016), and quantifying daily and annual PM concentrations in 102 cities (Andreão et. al., 2020). These studies showed satisfactory representation of meteorological variables but an overestimation of PM concentrations for some environmental company monitoring stations of São Paulo (CETESB), mainly in MASP. Albuquerque et al. (2018) used the Weather Research and Forecasting-Sparse Matrix Operator Kernel Emissions Models-3 Community Multiscale Air Quality Modeling System (WRF-SMOKE-CMAQ) to represent meteorological and air quality conditions over São Paulo, Brazil, and to evaluate the performance of the model (Albuquerque et al., 2018; Pedruzzi, et. al., 2019).

Accurate modeling of air pollution must consider atmospheric aerosol processes. The effects of aerosols on meteorological processes and air quality depend largely on their size distribution, chemical composition, mixing state, and morphology (Seinfeld and Pandis, 2016). This is particularly valid for smoke particles in the atmosphere over South America that are annually released from vegetation fires and represent a major aerosol source during the burning season (Hoelzemann et al., 2009). In the vicinity of megacities, urban industrial emissions may be predominant, but on a continental scale sources are mainly composed of carbonaceous aerosol emissions and trace gas emissions from deforestation and savanna maintenance fires. Hundreds to thousands of vegetation fires, primarily in *Cerrado* and Amazon forest ecosystems, emit vast amounts of aerosol particles into the atmosphere during the burning season and the aerosol effects by fires may go far beyond the local scale and significantly affect the hydrological cycle on a regional scale (Setzer and Pereira, 1991; Artaxo et al., 2005, Freitas et al., 2005, 2007a, Hoelzemann et al., 2009). If meteorological conditions are favorable, smoke plumes can be injected into altitudes above the planetary boundary layer (Andreae et al., 2001; Freitas et al., 2007b). Emissions generated from biomass burning contribute extensively to the global budget of several atmospheric constituents such as aerosols, carbon dioxide (CO_2), carbon monoxide (CO), nitrogen oxides (NO_x) and methane (CH_4), amongst others. Hence, fire emissions need to be modeled by global systems that monitor and forecast atmospheric composition, such as the European Copernicus Atmosphere Monitoring Services (CAMS) (Kaiser et al., 2012) and the included in the emission inventories that deliver emission fluxes to the CTM's.

According to Crippa et al. (2018), global emission inventories coupled with CTMs are useful tools to tackle these regional and global aspects, complementing air pollution measurements that provide information on local and regional air quality impacts. Emission inventories tabulate emission rates from individual sources and source categories for the pollutants of interest (Molina and Molina, 2002). Several global emissions inventories have been developed in recent years such as (Monitoring Atmospheric Composition and Climate (MACCity) by Granier et al. (2011), the Hemispheric Transport of Air Pollution Inventory (HTAP v2.2) by Janssens-Maenhout et al. (2015), the Community Emission Data System (CEDS) by Hoesly et al. (2018), the inventory based on Greenhouse Gas and Air Pollution Interactions and Synergies (GAINS), ECLIPSE V5a global emission fields by Klimont et al. (2017) for particulate matter, and the

Emissions Database for Global Atmospheric Research (EDGAR) for air pollutants and greenhouse gases calculated in a consistent and transparent way (Crippa et al., 2018).

In the environment of urban areas, the vehicular emissions are becoming increasingly important (Andrade et al., 2017; Ibarra-Espinosa et al., 2018) and measurements have shown that compounds emitted from vehicular exhausts can be highly reactive in the atmosphere, contributing to critical episodes of photo-chemical smog (Nogueira et al., 2015). Although emission inventories are an essential tool for managing and regulating pollution, large uncertainties in emission rates, temporal cycles, spatial distribution, and source identification often confound the development of cost-effective control strategies (Molina and Molina, 2002). In the urban centers of Brazil, the rapid economic growth triggered the increase of the vehicle fleet and therefore increased air pollution (Faiz et al., 1996; Miranda et al., 2012, Andrade et al., 2017; Ibarra-Espinosa et al., 2018). Studies about air quality and its effect on climate and human health for the MASP have been conducted since the 1970s. According to Andrade et al. (2015), in 1960, there was a decrease of air quality with high concentrations of pollutants emitted by industrial activities in the state of São Paulo without any control strategies on the emissions of air pollutants.

The MASP is the largest metropolis in South America, with a population of more than 21 million inhabitants. MASP includes 39 cities covering a surface area of approximately 8000 km^2 (IBGE, 2019). The climate in the MASP is characterized by temperate oceanic climate (*Cfb*) with wet (October to April) and dry (May to September) seasons. January and June are the hottest and coldest months of the year, respectively (Miranda et al., 2012). MASP suffers from severe air pollution from particulate matter of 10 μm (PM10) as well as 2.5 μm (PM2.5), Ozone (O_3) and aldehydes (Molina and Molina, 2004). During austral winter, unfavorable conditions for pollutant dispersion have been observed, since shallow inversion layers trap pollutants within the lowest 200-400 m height for several days resulting in elevated pollutant concentrations (CETESB 2009, 2017). In comparison with other urban areas of Brazil, the MASP has the best network of air quality monitoring stations, which provide data with the highest spatial resolution by the São Paulo State Environmental Sanitation Technology Company (CETESB) (Andrade et al., 2015).

The objective of this study is to adapt and provide a powerful air quality analysis to investigate the spatial and temporal variability of PM10 and PM2.5 simulated by EURAD-IM during July 10-13, 2016, during the dry season in Southeast Brazil, and October 22-25, 2016, during the transition season from dry winter to wet summer. The EURAD-IM was statistically evaluated and compared to the modeled results on a 1 km^2 grid resolution with CETESB surface monitoring stations of PM10 and PM2.5, as well as qualitatively with available Lidar profiles. In addition, the model was used to study the regional transport of pollutants to MASP. The period chosen for modeling is related to available observational data in MASP and allows to verify if the EDGAR emission inventory was representative. Meteorological fields were modeled using the Weather Research and Forecasting model (WRF, Skamarock et al., 2008), using three nested domains with 25-km, 5-km, and 1-km horizontal grid resolution, which covered the whole southeast of Brazil, São Paulo state, and MASP, respectively.

2. Model and data description

In this section the EURAD-IM air quality model, its respective input data, such as pollutant emissions and meteorological fields are described. Also, the observational data set that has been used to evaluate the model performance over the MASP is presented.

2.1 The Meteorological Driver model WRF

The WRF Advanced Research (ARW) model, version 3.7, is used to create the meteorological input for EURAD-IM. The WRF model is fully compressible non-hydrostatic and solves the meteorological equations on a Eulerian grid (Skamarock et al., 1994). The horizontal grid is the 'Arakawa C' grid (Arakawa and Lamb, 1977). The meteorological initial and boundary conditions are obtained from United State National Center for Environmental Prediction (NCEP)/National Center for Atmospheric Research (NCAR) Global Forecast System (GFS) at 0.25° resolution, including Newtonian nudging every 6h (https://rda.ucar.edu/datasets/ds083.2/).

In this work, three off-line model domains were used as can be seen in **Fig. 1a**, the coarse model grid encompasses the major south eastern region of Brazil around São Paulo with 25 km horizontal resolution (domain01). The 5 km resolution domain (domain02) covers the state of São Paulo (SP) while the 1 km resolution domain (domain03) is centered on the MASP at 23.55° S and 46.63° E. The domain01 has 110 × 101 grid points covering an area of 2750 km × 2525 km, domain02 has 326 × 241 grid points covering an area of 1630 km × 1205 km, and domain03 has 351 × 251 grid points covering an area of 351 km × 251 km, three domains with a vertical resolution of 35 layers up to 100hPa. **Fig. 1b** shows the topography of São Paulo characterized by flat land, hills, mountains, plateaus and depressions. An important hub connecting São Paulo, Minas Gerais (MG) and Rio de Janeiro (RJ) is the *Vale do Paraíba* (or Paraíba Valley). It is an important passage for commodities, industries and services in the depression between *Serra da Mantiqueira* and *Serra do Mar*.

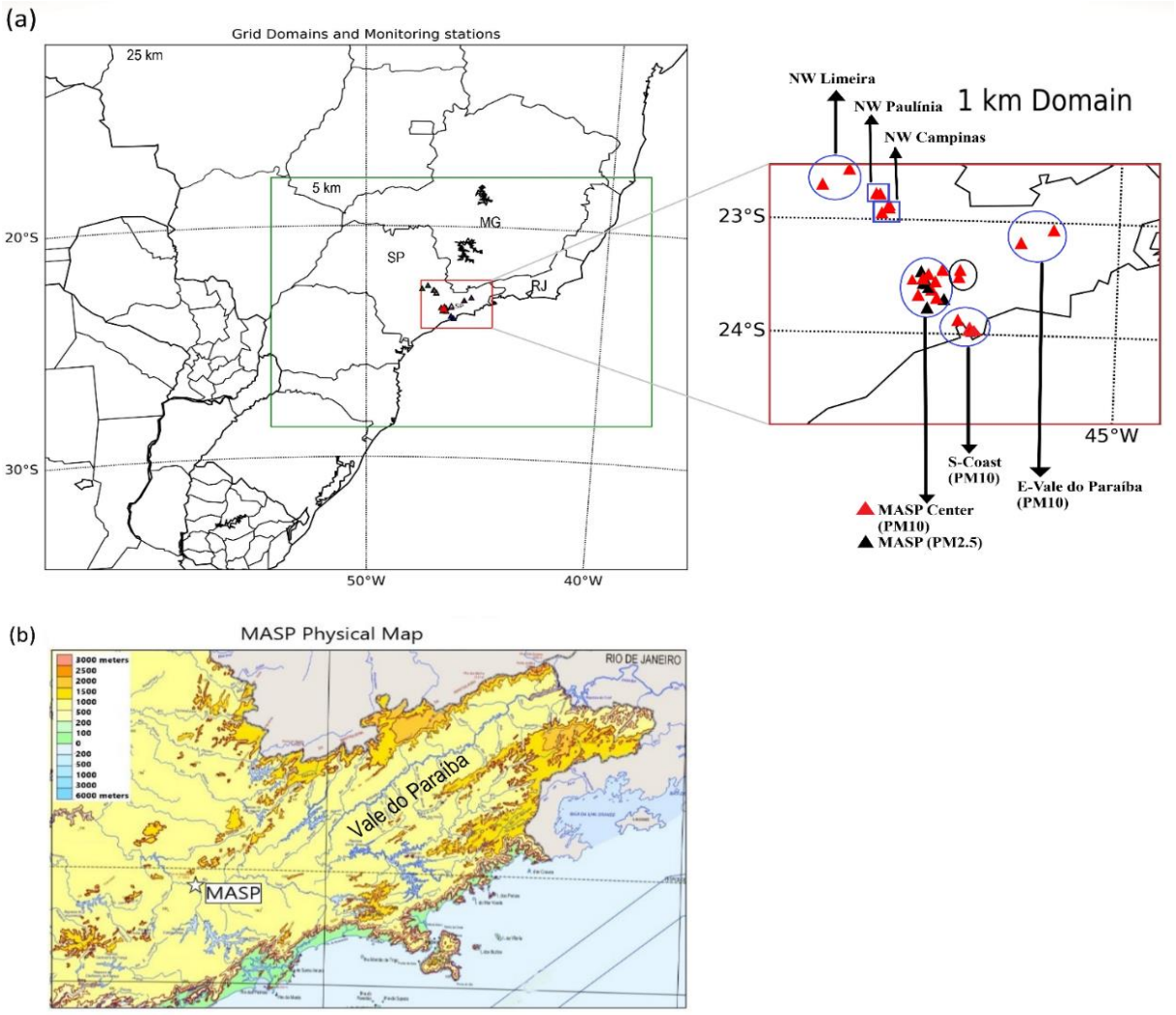

Fig. 1. (a) Allocations of the domains used in the EURAD-IM simulations, the red triangles are PM10 station and black triangles are PM2.5 stations from CETESB locations used in this study, (b) São Paulo physical map. Source: IBGE (2020).

The main physics parameterizations were chosen based on previous studies such as Andrade et al. (2015), Vara-Vela et al. (2018), Alburquerque et al. (2018; 2019), and Andreão et al. (2020a; 2020b) who focus on the region over South America/São Paulo performing air quality simulations. In our simulations the model physics include the Grell 3D ensemble scheme for convection (Grell and Freitas, 2014), the YSU scheme (HONG et al., 2006) for the boundary layer parameterization, WRF Single-Moment 3-class Scheme for the parameterization of cloud microphysics (Hong et al., 2004), the NOAH scheme (Tewari et al., 2004) for land surface processes, the RRTM scheme (Mlawer et al. 1997) for longwave radiation and the Dudhia scheme (Dudhia 1989) for shortwave radiation. The meteorological initial and boundary conditions were obtained from GFS meteorological data with 0.25° x 0.25° resolution.

2.2 The EURAD-IM Air Quality Model

The EURAD-IM has been developed to run simulations of meteorological processes, atmospheric chemistry, aerosol dynamics and transport on a regional scale. It is a mesoscale chemistry transport model

(Elbern et al., 2007) using WRF as offline meteorological driver. It is used for simulations focusing on emissions and their influence on air quality (Memmesheimer et al., 2000; Memmesheimer et al., 2004) as well as for operational forecast down to local scale using the nesting technique. Also, EURAD-IM can be used for episodic scenario forecasts focusing on special aspects of air quality simulations (Ebel et al., 1997; Huijnen et al., 2010, Monteiro et al., 2013, Marécal et al., 2015; Gama et al., 2019) and their analyses using chemical data assimilation and inverse modeling techniques (Elbern et al., 2000; 2007; 2010). The main relevant parts of the forward model are the EURAD Emission Model EEM (Memmesheimer et al., 1991, with later developments), and the kinetic preprocessor, which solves the equations for gas phase chemistry (KPP) (Damian-Iordache, 1996).

To propagate a set of chemical constituents forward in time EURAD-IM solves a system of partial differential equations (Elbern et al. 2007)

$$\frac{\partial c_i}{\partial t} = -\nabla(\acute{v} c_i) + \nabla(\rho K \nabla \frac{c_i}{\rho}) + A_i + E_i - S_i, \quad (1)$$

where c_i, $i = 1, \ldots, n$ is the mean mass mixing ratios of the n chemical species, $\acute{v}$ is the mean wind velocities, K is the eddy diffusivity tensor, ρ is the air density, A_i is the chemical generation term for species i, and E_i and S_i describe emission and removal fluxes, respectively.

The Eulerian chemistry transport model applies an operator splitting technique (McRae et al., 1982), where each process in **(1)** is treated independently in a sequence. In that way different numerical methods, which are specific for the physical character of the processes, can be used efficiently. EURAD-IM uses a symmetric splitting of the dynamic procedures, encompassing the chemistry solver module C (see Hass, 1991),

$$c_i^{t+\Delta t} = T_h T_v D_v C D_v T_v T_h c_i^t, \quad (2)$$

where T_h, T_v and D_v denote transport and diffusion operators, respectively, in horizontal (h) and vertical (v) directions. The emission term is included in C, the spatial discretization indices are omitted here. Concentration changes due to cloud effects are calculated at hourly intervals. During the cloud lifetime of one-hour aqueous phase chemistry and scavenging effects are integrated with time steps limited by these specific processes.

The CTM uses the aerosol module Modal Aerosol Dynamics model (MADE) (Ackermann, 1997; Ackermann et al., 1998), which is derived from the Regional Particulate Model (RPM) (Binkowski and Shankar, 1995). The aerosol size distribution is represented by three log-normal modes, I. e. - Aitken (d< 0.1 μm), accumulation (0.1 < d < 1 μm), and coarse (d > 1 μm) mode with standard deviations of σ_{Aitken} = 1.7, $\sigma_{Accumulation}$ = 2.0, and σ_{coarse} = 2.2, respectively. The chemical species treated in the finer aerosol modes are secondary inorganic components (sulfate, nitrate, and ammonium), secondary organic components of biogenic or anthropogenic origin, primary organic carbon, elemental carbon, and other unspecified material of anthropogenic origin. The coarse mode species include sea salt, wind-blown dust, and other unspecified material of anthropogenic origin. The anthropogenic component of the coarse particles is most often attributed to industrial processes (Ackermann, 1997; Ackermann et al., 1998). Each aerosol mode is subject to wet and dry deposition. The chemistry mechanism for the gas-phase is the RACM-MIM, developed by Geiger et al. (2003). It is based on the Regional Atmospheric Chemistry Mechanism (RACM) (Stockwell et al. 1997) mechanism combined with the Mainz Isoprene Mechanism (MIM) (Poeschl et al., 2000) and reflects an

advanced description of the air chemistry of biogenic ozone precursors. It treats 84 chemical species (as real species and condensed species classes) and contains 23 photolysis reactions and 221 chemical reactions of higher order.

2.3. Emissions

The EURAD Emission Module (EEM) prepares emission data for chemistry-transport-calculations. The EEM acts as an interface between the emission inventories available for certain areas and time periods to be simulated in the CTM. The EEM projects the emission inventory data spatially on to the numerical grid and computes the desired emission rates with a temporal resolution of one hour. The emissions are transformed from the original grid to any EURAD-IM grid and dis-aggregated to the source of the emission, if available. The variability of emissions due to seasonal, weekly, or daily cycles is incorporated in EEM output using hour-of-day, day-of-week, and monthly emission factors to distribute the total annual emissions temporally as described in Simpson et al. (2012). For a more detailed description see Memmesheimer et al. (1995).

In this study the EDGAR inventory v4.3.2 (Crippa et al., 2018) was used. EDGAR covers gaseous air pollutants of Carbon Monoxide (CO), Nitrogen Oxides (NOx), Sulfur Dioxide (SO_2), total Non-Methane Volatile Organic Compounds (NMVOC) and ammonia (NH_3). As to the aerosols PM10, PM2.5, and carbonaceous species BC and OC are provided. Its database was built considering the location of power and manufacturing facilities, road networks, transportation routes, human and animal population density, and agricultural land use, which vary over the years. Country emissions are then compiled considering the International Energy Agency (IEA) energy statistics. The total national emissions are gridded using population, road, power plants, animals, and crop proxy data. Air quality modeling using EDGAR was performed with focus on primary particles (PM10, PM2.5) for the three domains with 25 km, 5 km and 1 km horizontal resolution. The EURAD-IM uses MADE to calculate initial number concentrations from given mass concentrations and from there calculates the minimum median diameters of the particles. The aerosol chemistry encompasses the formation of secondary aerosols formed by gas-to-particle conversion of inorganic and organic precursors. The formation and partitioning of secondary organic aerosols (SOA) are simulated by the Secondary ORGanic Aerosol Model (SORGAM) coupled to MADE. In the case of elemental carbon, organic carbon, and other fine particles of anthropogenic origin emissions are compiled from land-use characteristics and emission inventories (in this case, EDGAR) and delivered for each model grid. They are subject to seasonal, weekly, and diurnal variations. Additionally, the EURAD-IM calculates mineral dust emissions and sea salt emissions out of the turbulent flux using the parameterization of Monahan (1988) is used, which estimates the flux depending on the particle size.

All emissions are split across a set of emission source sectors defined by the Selected Nomenclature for Air Pollutants (SNAP) as described in **Table 2.** Here, SNAP 10 is assigned to agricultural emissions, describing all anthropogenic emissions from this sector including on-site burning of residue from main crops harvested for dry grain (such as soy), burning of sugar cane crop residue and on-site burning of residue from crops not mentioned above.

Table 2.

SNAP source sectors (Eurostat, 2004).

SNAP 1	Combustion in energy and transformation industries
SNAP 2	Residential and non-industrial combustion
SNAP 3	Combustion in the manufacturing industry
SNAP 4	Production processes
SNAP 5	Extraction and distribution of fossil fuels
SNAP 6	Solvent and other product use
SNAP 7	Road transport
SNAP 8	Other mobile sources and machinery
SNAP 9	Waste treatment and disposal
SNAP 10	Agriculture

2.4 Chemical Initial and Boundary Conditions

To obtain realistic initial conditions for the EURAD-IM simulations, a model spin-up of three days was performed, starting from Copernicus Atmosphere Monitoring Service (CAMS) fields (Inness et al., 2019) to provide realistic three-dimensional analysis for initial values for the desired episodes. CAMS is the latest global reanalysis dataset of atmospheric composition produced by the European Center for Medium-Range Weather Forecast (ECMWF) consisting of three-dimensional time-consistent atmospheric composition fields, including aerosols and chemical species. CAMS provide global analysis and forecasts of atmospheric composition, alongside European air quality forecasts (Hollingsworth et al., 2008) using the CAMS Integrated Forecasting System (C-IFS) model (Morcrette et al., 2009; Benedetti et al., 2009; Peuch and Engelen, 2012; Flemming et al., 2015).

Boundary values for the nested grids are obtained from their respective mother grids. From available measurements of the transported species latitude-dependent vertical profiles are derived and equally distributed over the whole model domain. For the coarsest grid, chemical boundary conditions of the EURAD-IM model also use CAMS reanalysis, based on global emission datasets that include anthropogenic emissions from the Monitoring Atmospheric Composition and Climate/CityZen (MACCity) inventory (Stein et al., 2014) and biomass burning emissions from the Global Fire Assimilation System (GFAS) data set (Kaiser et al., 2012). Great care has been taken to ensure that the emission datasets used in CAMS were consistent in time and that consistent anthropogenic, biogenic and biomass burning emissions were used in the aerosol and chemistry modules (Inness et al., 2019).

2.5. Observational data

The EURAD-IM model is validated against observational in-situ data from the operational monitoring network of the São Paulo state environmental agency CETESB and a Lidar which are introduced in the following. **Fig. 1a** shows the locations of the CETESB stations and the Lidar.

2.5.1 CETESB in situ data

In 2016, CETESB operated 60 fixed automatic stations, out of which 29 stations were located within the MASP, while the others 31 stations are distributed in the inland and at the coast. These stations measure concentrations of PM10, PM2.5 as hourly means. The method used by CETESB's automatic monitoring stations to measure the concentration of PM suspended in the atmosphere is absorption by beta radiation. This measurements technique is widely used for operational use as it provides a high accuracy. In this study, 20 sites of PM10 and 5 sites of PM2.5 CETESB automatic station were used to evaluate and compare with model results for a 1 km domain, as shown in **Fig. 1a**. Neighboring stations, which are assumed to be exposed to a similar chemical regime, were grouped into 8 clusters of super-observations (**Table S1**). Further, the Pearson's correlation coefficient, RMSE and Bias for each cluster were calculated.

2.6. Characterization of the case studies

Two case studies were carried out. The first one during the wintertime (characterized as dry season), for the days of July 10-13, 2016, and the second one during the springtime (transition to wet season), for the days October 22-25, 2016, in southeastern Brazil. During most of the dry season in SP state, frequent subsidence and thermal inversion layers provide unfavorable conditions for the dispersion of pollutants (Alburquerque et al., 2012) and biomass burning emissions are transported from different parts of Brazil and South America (Hoelzemann et al., 2009, Miranda et al., 2017; Vara-Vela et al., 2018) to the south and southeast Brazil. During spring in southeastern Brazil, the rains become more intense and frequent, marking the transition period between the dry season and the rainy season.

According to CETESB (2016), the year 2016 was marked by a neutral situation of oceanic and atmospheric conditions in the Equatorial Pacific region, indicating the end of the global scale phenomenon El Niño-Southern Oscillation (ENSO) that had acted throughout 2015 and lead to atmospheric blockings, both in the Pacific and in the Atlantic Ocean. The latter influenced the rainfall regime, varying between very rainy months and dry and hot months in the State of São Paulo. In contrast to the situation in 2015, July and September 2016 were, in general, more wet than the climatological average (CETESB, 2016). The year 2016 was marked by favorable weather conditions for the dispersion of air pollutants. According to data from CETESB, the period from May to September is generally the most favorable for high pollution episodes as the free dispersion of primary pollutants in the State of São Paulo is hampered by a very stable atmosphere and frequent thermal inversion events. In winter 2016, only 25 days were counted as favorable for pollution episodes which is the lowest in the last ten years (CETESB, 2016).

Significant events of long-range and regional transport of aerosols into the MASP are often observed, especially during the winter period of South America. Two of the 2016 aerosol transport events

coincided with local measurements of aerosols properties by the Lidar of MASP and CETESB surface station data. The first event occurred from July 10–13 during the dry season and the second from October 22–25 during the onset of the wet season. Both events show distinct meteorological conditions that contribute in very different ways to increase air pollution concentrations in the MASP.

3. RESULTS AND DISCUSSION

3.1. Case study July 10–13, 2016: Dry season in Southeast Brazil

The statistics indices obtained from the comparison between hourly observed and modeled meteorological parameters are presented in section S6: "Meteorological validation" in the supplementary material. **Fig. 2** shows the meteorological situation on the 25 km model domain for July 10-13. It is important to note that the wind speed and direction at 850 hPa (about 1400 m a.g.l.) indicate air masses coming from the Amazonian basin associated with the South American Low-Level Jet (SALLJ). The SALLJ is an important driver of long-range transport of pollutants to South and Southeast Brazil (Freitas et al., 2005; Freitas et al., 2007; Vera et al., 2016; Martins et. al., 2017). Most of the SALLJ passed over and through São Paulo towards the Southern Atlantic Ocean during this first case study.

Since July 10, São Paulo state had been under the influence of a closed high-pressure system of approximately 1022 hPa **(Fig. 2a).** While a previous low-pressure system was moving east from the southern Atlantic to the south of Brazil, a second one was arriving from Bolivia and Paraguay with a central pressure of about 998 hPa (**Fig. 2b)**. This synoptic condition was accompanied by deep convection systems in São Paulo state. The associated high-pressure system was not so strong over the continent during the following days over the region (**Fig. 2c** and **Fig. 2d)**. A second extratropical cyclone coming from the Pacific Ocean passed the Andes Mountains cordillera at the latitude of 22° S and built a new cold front over the Atlantic Ocean that extended its influence over the continent at latitudes of the southern region of Brazil on the days of July 12-14. The low-pressure system moved quickly to the east and the SALLJ lost its configuration in the following hours. The wind magnitude over MASP was about 10 m/s and wind direction represented by wind barbs at 850 hPa were pointed to the Southeast reaching the MASP, which means that the SALLJ affected MASP in that case.

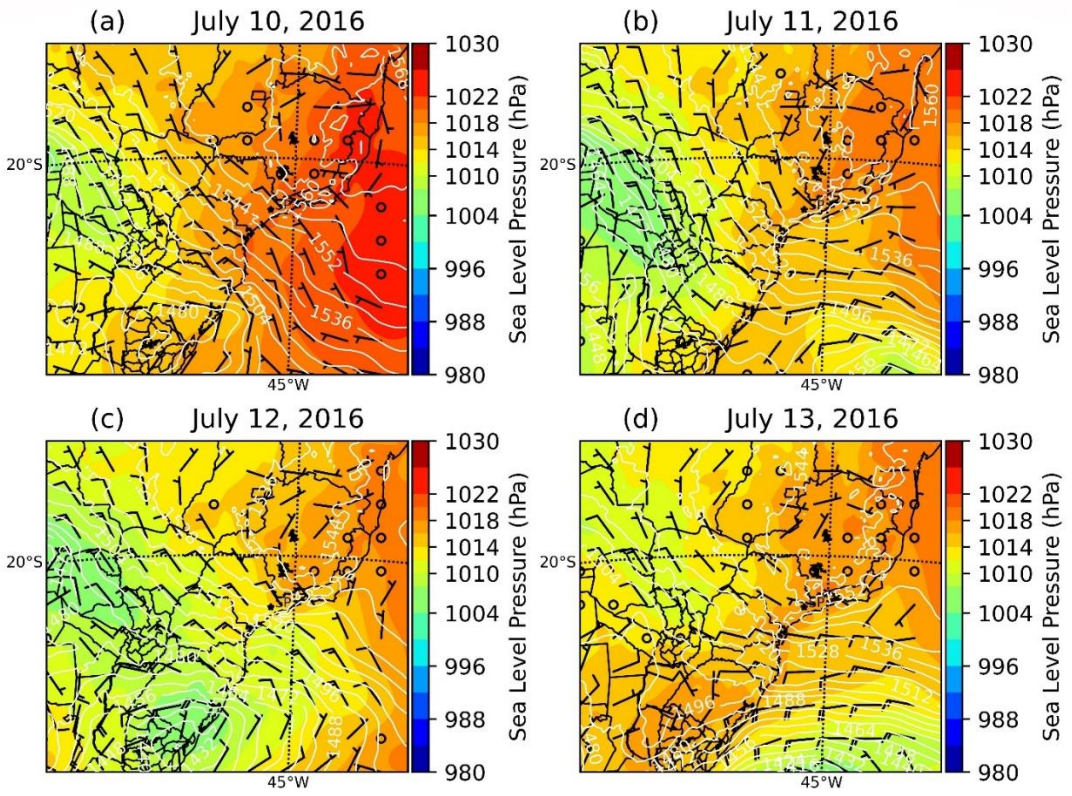

Fig. 2. Sea level pressure (hPa) (color code jet), wind (m/s) at 850 hPa and Geopotential height (m) at 850 hPa represented by the white lines simulated by the WRF for July **(a)** 10, **(b)** 11, **(c)** 12, and **(d)** 13, 2016, daily average on the 25-km resolution grid**.**

Fig. 3a and **Fig. 3b** present the Aerosol Optical Depth (AOD) from Terra and Aqua (MYD04_L2) satellites at 3 km resolution for day time overpasses (Levy et al., 2013), Suomi National Polar-Orbiting Partnership (S-NPP) the merged dark target/deep blue AOD layer (Sayer et al., 2017) as well as the MODIS fire hotspots products from the Terra (MOD14) and Aqua (MYD14) satellites for July 11 and 12, 2016. **Fig. 3a** and **Fig. 3b** show the tropospheric AOD column varying between 0–3 over São Paulo state, reaching a value of 5 over the Southeast Atlantic Ocean and Central Brazil. High values of AOD in central Brazil are in the same location as the high number of fire counts, which indicates relation to aerosol load from biomass burning origin.

On July 12, the fire hotspots were most abundant in Central Brazil, a region between the states of Goiás (GO), Tocanctins (TO) and the Federal District (DF), with predominant *Cerrado biome*. *Cerrado* is the second most extensive vegetation formation in South American, with an area of more than 2 million square kilometers (IBGE, 2016). Its area represents one fourth of Brazil's entire land surface. According to data from INPE for 2016, the *Cerrado* had approximately 151.142 km^2 of its area burnt, whereas a total area of 280.970 km^2 burnt in the whole country. For the month of July, the total area burned at *Cerrado* was 21.514 km^2, while in the Amazon, it was 4.514 km^2 (INPE, 2016). This biomass burning activity in Central Brazil has a significant impact on the long-range transport of air pollutants to and across Southeast Brazil.

The state of São Paulo also presented biomass burning activities in its center, northwest of the MASP. The aerosols emitted by these fire activities, reached higher levels of the atmosphere (up to 500 hPa) and are

transported to regions more distant from their point of origin (Hoelzemann et al., 2009, Miranda et al., 2017; Vara-Vela et al., 2018). The state of São Paulo engages in intense sugarcane production, which is also associated with an annual burning process shortly before or during harvesting (Allen et al., 2009; Vasconcellos et al., 2010; Souza et al., 2014; Andrade, et. al., 2017). Although legislation has been prohibiting this practice along with general agricultural waste burning in the more recent years, it is still very common within the state of São Paulo throughout the year (e.g. Kumar et al., 2016).

Through the analysis of the Lidar vertical profiles it is possible to detect the different aerosols layers and their heights (see topic S1: "Methodology of Lidar profiles of aerosol properties for São Paulo"). Merging this information with an air quality model, it is possible to study the origin and the transport of aerosols in the atmosphere. **Fig. 3c** and **Fig. 3d** shows the mean vertical profiles of aerosol backscattering coefficients for 355 nm and 532 nm respectively for July 12, retrieved by applying the KFS inversion method to the data obtained from the SPU-Lidar system in the MASP. Both profiles show that most of the aerosol load in the atmosphere is concentrated within the PBL, approximately up to 2100 m (a.g.l.) showing a peak of 0.0017 $km^{-1}sr^{-1}$ at approximately 700 m. However, a very thin aerosol layer can clearly be seen above the PBL, between 4000–4700 m a.g.l. - which would typically be from a source outside the MASP. Typically, this type of intrusion is often related to biomass-burning aerosol transported from remote locations outside MASP. However, for this case the total column Lidar ratio at 532 nm is 56 sr and can be associated to less absorbing urban particles (Weitkamp, 2005).

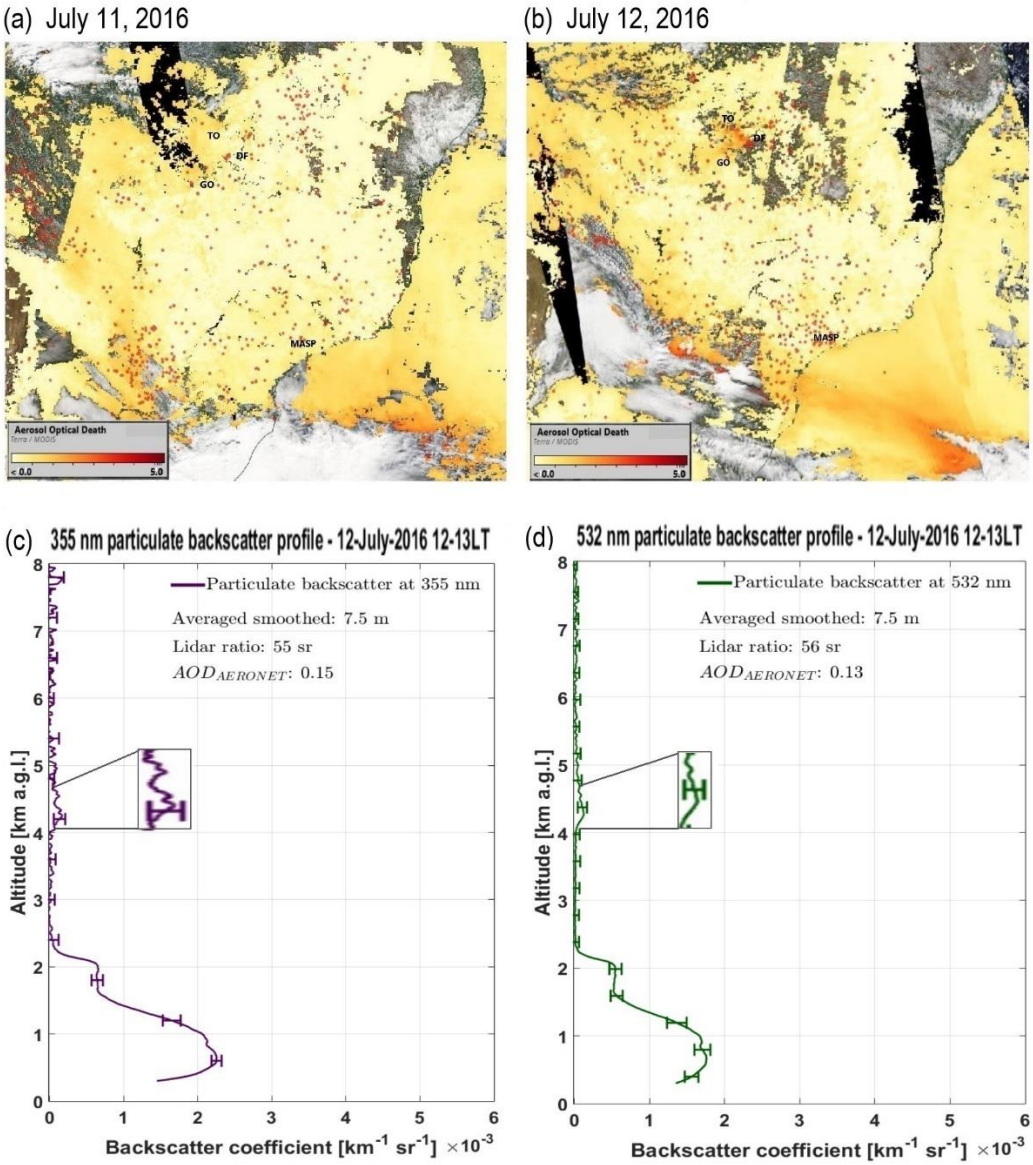

Fig. 3. (a) and **(b)** Compiled satellite AOD columns from Terra (MOD04_L2) and Aqua (MYD04_L2), Suomi NPP/VIIRS Deep Blue Aerosol Optical Depth layer, MODIS AOD (MOD04_3K) and Aqua (MYD04_3K) and associated MODIS fire hotspot products (red dots) for July 11 and 12, respectively (Source: NASA, 2020); The Backscatter profiles for July 12, 2016, between 1200 – 1300h LT from the IPEN Lidar in the MASP at: **(c)** 355 and **(d)** 532 nm.

EURAD-IM results on the 25-km domain at 850 hPa on July 12 1600 Local Time (LT) are presented as PM2.5 concentrations in **Fig. 4a** and PM10 concentration in **Fig. 4b**. On this day a plume located at latitude 18° S and longitude 50° W, which is at the border between the states Goiás (GO) and Brasília (DF), travelled about 700 km following the trajectory of the SALLJ and reached SP state. In **Fig. 4a** elevated PM2.5 concentrations of agricultural waste burning origin can be seen over Sao Paulo state. This plume mixed with the aerosol layer coming from the fires in central Brazil, forming a mixed aerosol layer on the way to the MASP.

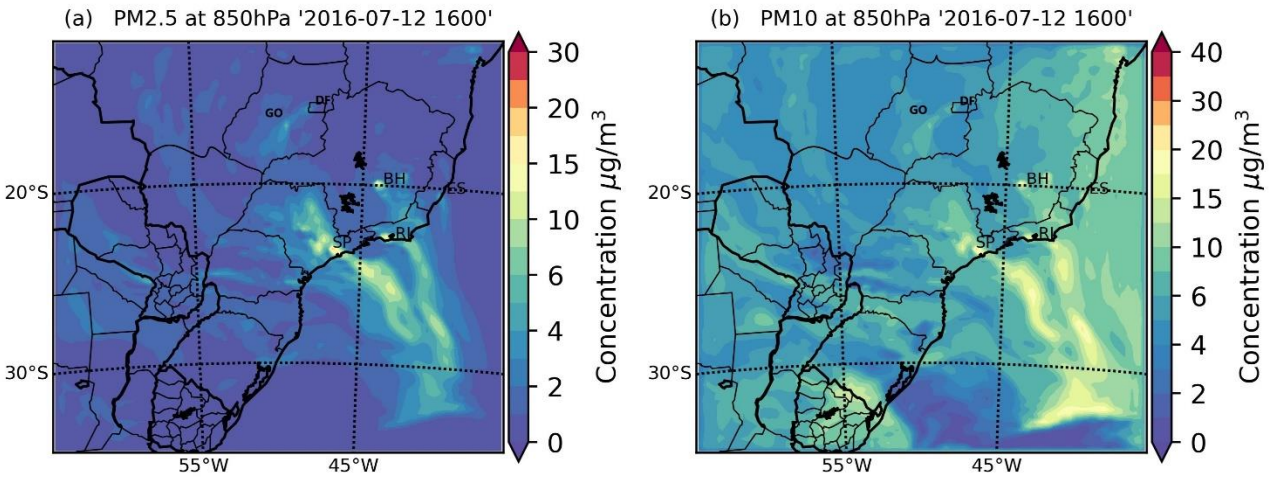

Fig. 4. Aerosols simulations of EURAD-IM on the 25-km domain **(a)** PM2.5 and **(b)** PM10 concentrations at 850 hPa on July 12, 2016 at 1600 LT**.**

Fig. 5a and **Fig. 5b** depict the PM2.5 concentrations as simulated by the EURAD-IM on the 5-km domain at 850 hPa, on July 12 and 13 at 0400 LT. The time was chosen for both days because they best represent the regional transport at 850 hPa coming from other regions of Brazil, **Fig. S1** presents simulation between July 12 0400 LT to July 13 1200 LT. **Fig. 5a**, in line with **Fig. 4**, indicates that the plume from Goiás and Brasília reaches the state of São Paulo. **Fig. 5b** shows the mixing of PM2.5 plumes produced by the MASP and the Metropolitan Area of Rio de Janeiro (MARJ) over the ocean. Thus, the SALLJ that passes through SP state not only transports pollution from Central Brazil to São Paulo but also transports pollutants to MARJ via the Atlantic coastal region between the states of São Paulo and Rio de Janeiro. The PM10 EURAD-IM simulations shows a similar behavior as those of PM2.5, which are shown in **Fig. S2**.

Fig. 5c and **Fig. 5d** show the PM2.5 concentrations at surface on July 12 and 13, respectively, at 0400 LT. The impact of agricultural waste burning emission in São Paulo state is more evident, reaching values of about 30 µg/m^3 at the municipality Ribeirão Preto (RP) and also at São José do Rio Preto (SJ), considered as an industrial and agricultural area in the State of SP according to CETESB (2016). EDGAR emissions showed a predominance of emissions of Agricultural activities (SNAP 10) and Waste treatment and disposal (SNAP 09) in the region (**Fig. S5**). The EURAD-IM simulations on the 5 km domain show that the resolution significantly affects the concentration of total PM2.5, especially the maximum and minimum values over the MASP, as model values represent an average of each grid cell's volume. **Fig. 5** also depicts significant impact of other urban centers such as the metropolitan regions as Rio de Janeiro and Belo Horizonte in the state of Minas Gerais on the PM concentrations. These urban centers yield high concentrations of both coarse and fine aerosols.

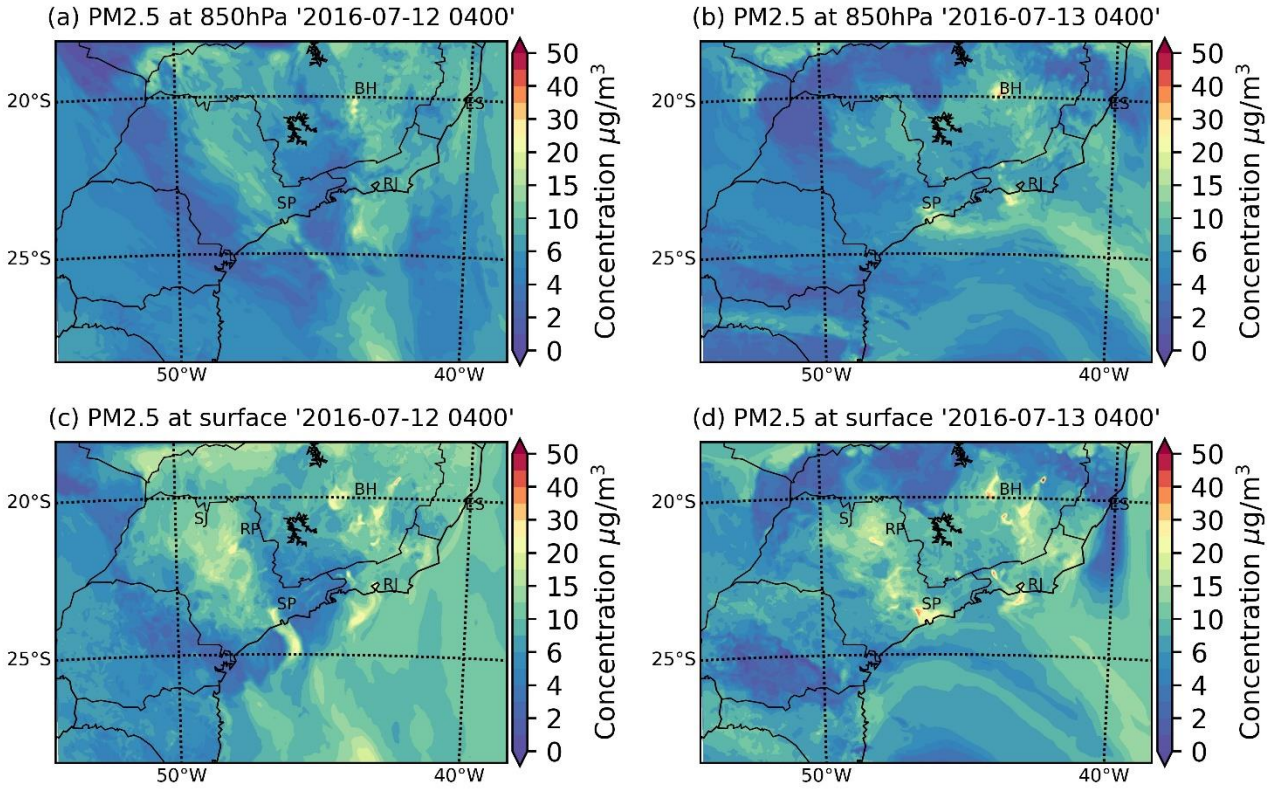

Fig. 5. PM2.5 concentration simulated by EURAD-IM with 5-km horizontal resolution at 0400 LT at 850 hPa on July 12 (a), and July 13(b) (top panels), and at surface on July 12 (c), and July 13 (d) (bottom panels).

Fig. 6 presents the PM2.5 concentrations on the 1-km domain at 850 hPa and at surface for July 12 and 13 at 0400 LT, respectively. At this resolution the higher PM concentrations transported by SALLJ can be clearly identified. July 12 at 0400 LT was chosen because it best represents the moment that pollutant plumes are reaching MASP through the SALLJ mix with pollution generated by the MASP during the day. On July 13, at 0400 PM2.5 plumes are being lifted over MASP and move to the direction of MARJ (**Fig. S1** and **Fig. S2** show July 12 at 0400 LT to July 13, 1200 LT for PM2.5 and PM10 at 850 hPa). The synoptic conditions for July 12 **(Fig. 2c**) show that wind direction at 850 hPa was pointing to southeast in the direction of the ocean and the low-pressure system was over the south of Brazil. On July 13 the low-pressure system moved over the ocean (**Fig. 2d**) changing the wind direction and favoring the displacement of pollutants from SP to RJ. The EURAD-IM results for the period of July 12 showed that the pollution generated by MASP, where industrial and vehicular emission were predominant. These pollutants are added to the pollution that originated from Central Brazil and the interior of SP state, where also intensive agricultural and industrial activities occur. The wind at 850 hPa reaching MASP is coming from the Northwest (Amazon Basin and Central Brazil, see **Fig. 2**). Downwind of MASP the plumes with elevated PM concentrations turn towards the Northeast or North where they are channeled through the Paraíba Valley or transported along the coast of São Paulo state to Rio de Janeiro state (**Fig. 6b**).

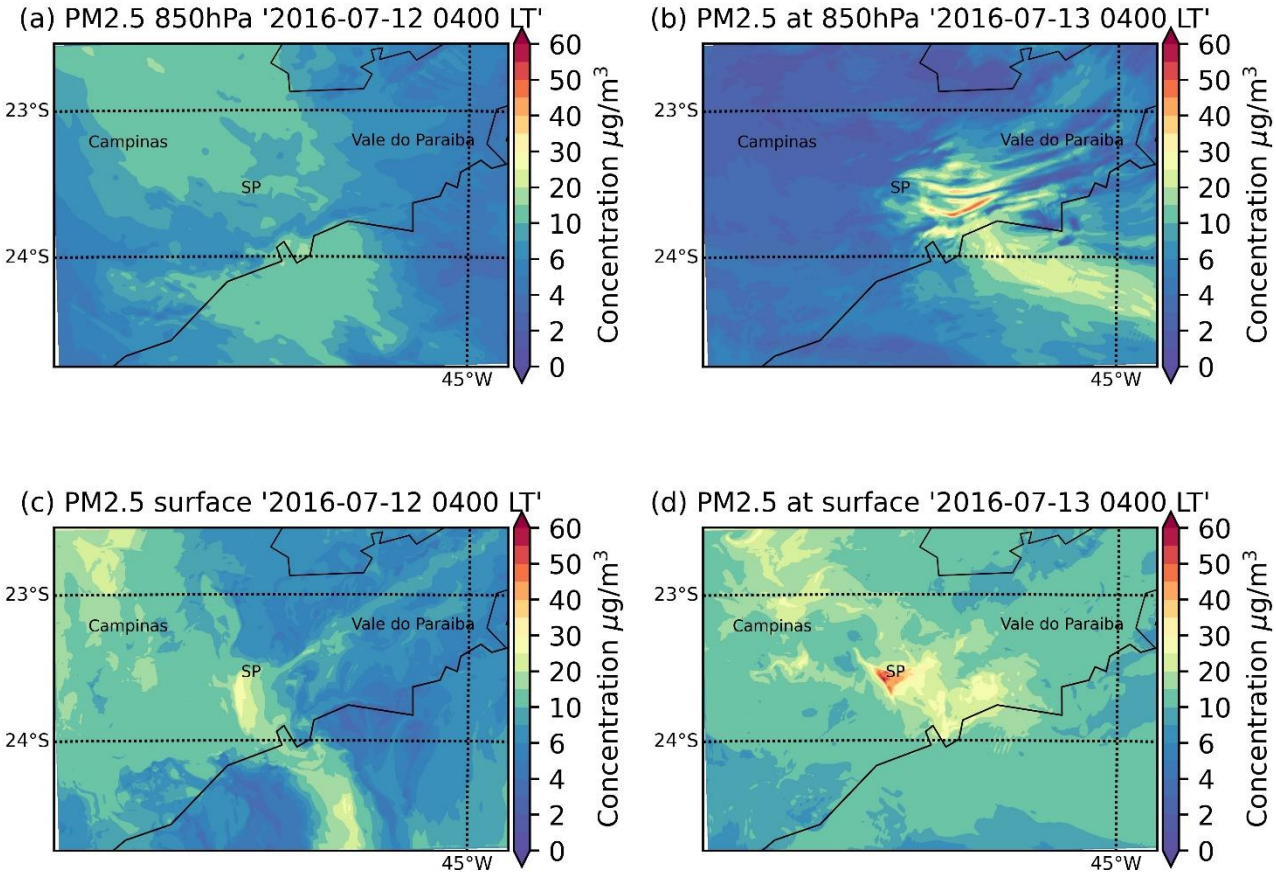

Fig. 6. PM2.5 concentrations simulated by EURAD-IM on the 1-km resolution grid at 850 hPa, 0400 LT for **(a)** PM2.5 on July 12; **(b)** PM2.5 on July 13 and at surface for **(c)** PM2.5 on July 12; **(d)** PM2.5 on July 13, 2016.

We extracted the concentration of total PM10 and PM2.5 at 850 hPa upwind the urban area of MASP, and assumed this value as roughly conserved when entering the city area: without significant time for deposition or a major amount of other components than biomass burning in the plume. We set the total PM, with the local city PM emissions added, in ratio to the upwind value. According to the wind speed and direction, we estimated that the contribution of PM10 from the interior of SP was 47 % of the total mass of PM10 in the city at 850 hPa for July 12-13, while for PM2.5 it was 50 %. Of this total PM10 at MASP, 13 % contributed to increase the concentration of PM10 in the of Vale do Paraíba advected by the winds and 30 % of total PM10 from MASP contributed to the increased PM10 over Santos. For PM2.5 the contribution was 21 % for Vale do Paraíba and 50 % for Santos.

Fig. 7 presents the comparison considering in-situ observations of PM10 and PM2.5 surface concentration at 26 CETESB stations and modeled EURAD-IM simulations at the coinciding 26 grid boxes of the 1 km domain. Neighboring stations, which are assumed to be exposed to a similar chemical regime, were grouped into 8 clusters of super-observations, according to Table S1. Further, the Pearson correlation coefficient, RMSE and bias for each cluster were calculated in **Table 3**.

Table 3

Model quality indicators calculated with hourly concentration observed/modeled from July 10-13 in 26 background sites (20 PM10 and 5 PM2.5) grouping in 8 Clusters according to **Table 1**.

Cluster	r	RMSE	Bias
MASP Center (PM10)	0.72	30.85	-37.70
MASP North (PM10)	0.50	17.95	-8.80
NW Paulínia (PM10)	0.55	26.12	-22.10
NW Campinas (PM10)	0.61	29.73	-35.50
NW Limeira (PM10)	0.50	30.04	-38.60
S-Coast (PM10)	0.68	16.75	-20.70
E-Vale do Paraíba (PM10)	0.67	18.35	-20.30
MASP (PM2.5)	0.38	20.77	-32.20

Table 3 presents statistical indexes for PM10 and PM2.5. At the surface level, the model reproduced the behavior of observed PM10 concentrations but underestimated the observations with a moderate positive Pearson correlation for clusters outside MASP CENTER. In the cluster MASP NORTH, S-Coast and E - VALE DO PARAÍBA - **Fig 7b, Fig 7c** and **Fig 7g**, the EURAD-IM were inside the standard deviation of observations presenting a correlation coefficient of 0.50, 0.68 and 0.67, respectively, which is a moderate positive relationship according to Wechsler (1996). The EURAD-IM performs especially well for the cluster MASP CENTER (**Fig. 7a**) where the observational grid is denser. The Pearson coefficient was 0.72, with a variance of RMSE = 30.85, and underestimated the observations (bias = -37.70). For PM2.5 Pearson's correlation was r = 0.36 at MASP with EURAD-IM underestimating the observations by (bias = -32.20) (more information about see topic **S5. Model Performance**, in the supplementary material). The model better represented the daytime PM10 concentrations, where more CETESB monitoring stations were available.

At S-Coast (see location in **Fig. 1**) EURAD-IM lies inside the standard deviation of the observations that for this area englobes the CETESB stations of Santos, Santos Ponta da Praia and Cubatão. This area is characterized as an important industrial area of the MASP and road transport is also a large source of pollution, which can dominate pollutant concentrations at ground level, depending on meteorological conditions. Dispersion is restricted by surrounding mountain ranges (Allen et al., 2009). The pollution generated by the port and industrial region of S-Coast is influenced by the sea breeze that transports this pollution at times to MASP through the sea-breeze front toward the center of the city (Freitas et al., 2005). S-Coast pollution can also be transported to regions as MARJ or southward and south-eastward along the Atlantic coast.

For the other clusters, the correlation varied between 0.5 to 0.7. The model also reflects the morning (0500 – 0900h LT) and the evening rush hour (1700 – 2000h LT) well, during which very high traffic emissions are the rule. Especially at the evening, after 1700 LT, the PM concentration increases for all cluster during

July 10-13, due to traffic emission and unfavorable weather condition for pollutants dispersion. For July 11, PM10 reaches a peak at 0100 LT for all clusters (C - MASP CENTER = 94 μg/m^3, E – MASP CENTER = 40 μg/m^3; C – MASP North = 65 μg/m^3, E – MASP North = 40 μg/m^3; C NW Paulínia = 108 μg/m^3, E – NW Paulínia = 44 μg/m^3; C - NW Campinas = 96 μg/m^3, E - NW Campinas = 41 μg/m^3; C - NW Limeira = 76 μg/m^3, E - NW Limeira = 50 μg/m^3; C – S-Coast = 80 μg/m^3, E – S-Coast= 49 μg/m^3; C – Vale do Paraíba = 76 μg/m^3, E - Vale do Paraíba = 57 μg/m^3) and for PM2.5 at MASP as well, C - MASP = 60 μg/m^3, E - MASP = 37 μg/m^3. Similar peaks of PM10 and PM2.5 concentrations occur for the following days in the evening after 1700 LT until later night (**Fig 7)**. The large number of vehicles circulating in the city at these times match with the low height of the PBL causing an increase in the concentration of PM10 and PM2.5. Those high concentrations measured by CETESB stations for this episode must be related not only with the traffic emissions and industrial activities but also with the biomass burning activity that happens during the dry season in the interior of SP state and also in the Amazonian basin and Central Brazil.

The results presented for July 10-13 are consistent with previous studies that show impact of the long-range transport of biomass burning on air quality in Southeast Brazil (Pickering et al., 1996; Hart and Spinfaiiae, 1999; Freitas et al., 2005; Silva Dias, 2006; Freitas et al., 2009; Rosário et al., 2013; De Oliveira et al., 2016; Martins et al., 2018), and the state of SP (Andrade et al., 2015; Kumar et al., 2016; Andrade et al., 2017). However, within MASP the main sources of anthropogenic emissions remain industrial and traffic (Andrade et al., 2017; Vara-Vela et al., 2016; Ibarra-Espinosa et al., 2018). According to EDGAR emissions used for this work, for the MASP the combustion in the manufacturing industry (SNAP 03) are major emitters of PM10 (89 % of total emission of PM10), and of PM2.5 with 40 % of the total emission of PM2.5 in the MASP, while road transport (SNAP 07) with others mobile sources and machinery (SNAP 08) are responsible for 38 % of total PM2.5 emissions (more information about emission per sector in the supplementary material **Table S2**). The model results show the complex vertical structure of PM concentrations over MASP enabling to distinguish PM from these two main source regions. In addition, it is noted that for these days the concentrations exceeded the threshold of PM10 of daily 50 μg/m^3 established by WHO. The maximum concentration occurred in C – MASP North on July 13 at 2200 LT, with a measured average concentration of PM10 of 147 μg/m^3 while EURAD – MASP North calculated 64 μg/m^3.

In all cluster inter-comparisons for this episode in July the EURAD-IM simulations under-estimate the measured values in many cases by the order of 10 – 40%, especially when local concentration maxima occur. However, large differences between the measured concentration at individual sites within the clusters can also be observed in NW PAULÍNIA, NW CAMPINAS, NW LIMEIRA, **Fig 7d-f**, respectively. The EURAD-IM model is not optimized for inner city air quality, as its regional scale is not representative comparing to individual monitoring stations within the city. Therefore, short concentration peaks produced by very local emissions cannot be reproduced by EURAD-IM. The EDGAR emissions, since they are based on the year 2012, use emission factors based on international statistics in their estimates (IPCC, 2006a). The EDGAR inventory needs to be updated and improved. For the MASP, Ibarra-Espinosa et al. (2018), showed that VEIN estimates for CO were more than 20 times higher than corresponding EDGAR emissions, showing that EDGAR may underestimate PM10 and PM2.5 as well.

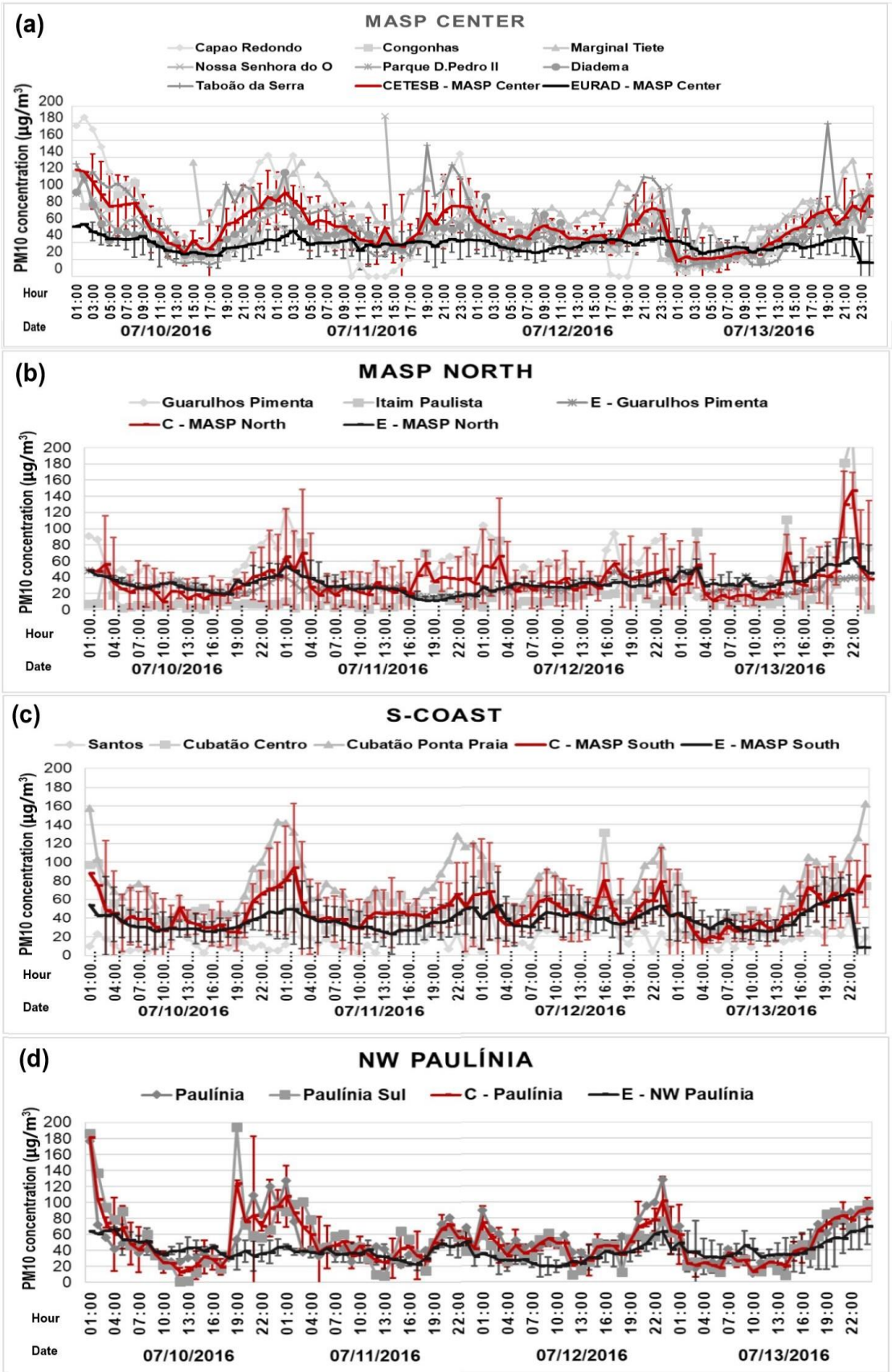

Fig. 7. PM10 concentrations for July 10 to 13, 2016 as measured by CETESB stations and modelled by EURAD-IM. For each CETESB super-observation (red) the original data at the observation sites (grey) and EURAD-IM super-observation (black) are given. Further, Table 3 defines the cluster grouping.

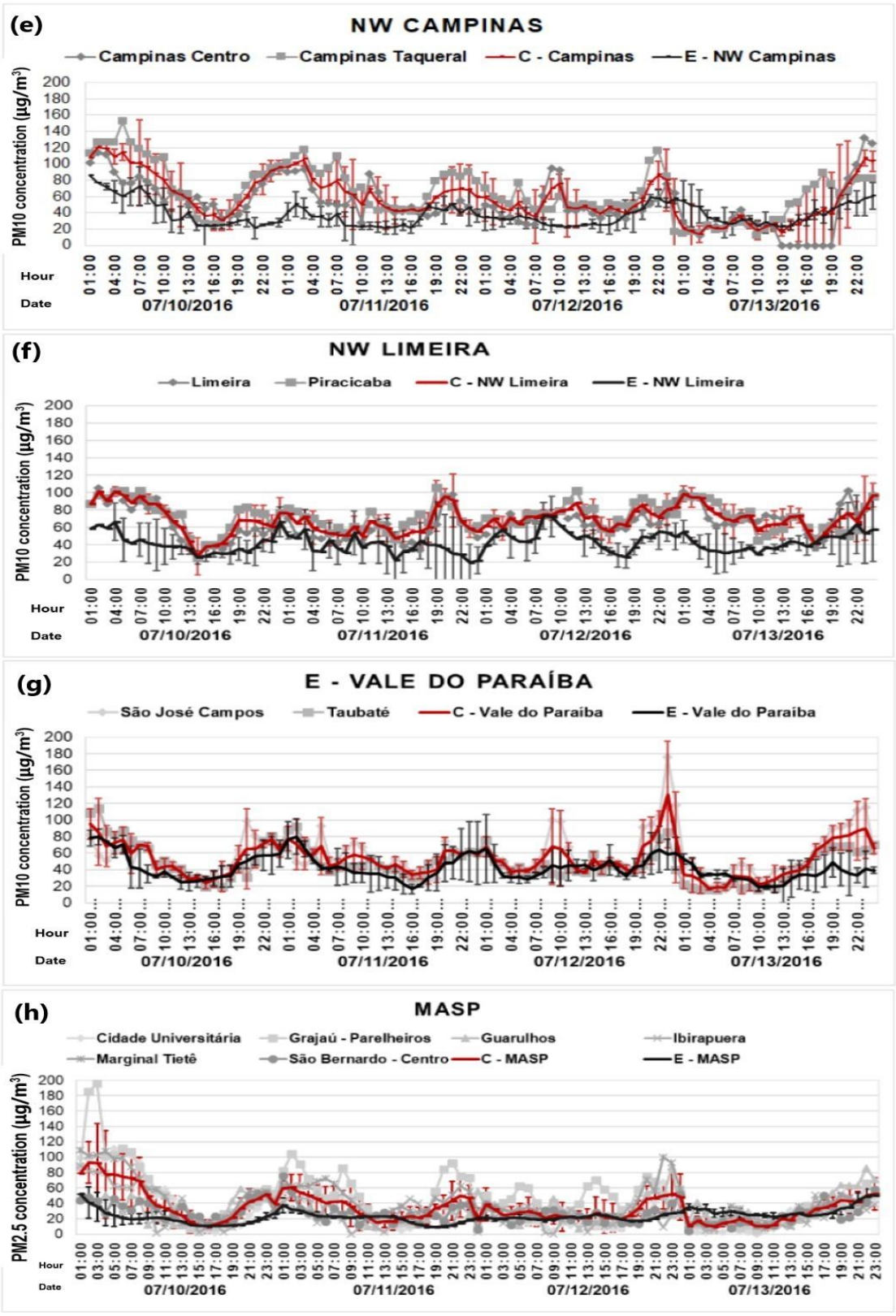

Fig. 7. Continued.

3.2. Case study on October 22–25, 2016: Transition season from dry winter to wet summer in southeastern Brazil

As a second study, PM concentrations in the period of October 22-25 are analyzed. The predominant synoptic situation during this second event is more complex than during the first event (**Fig. 8)**. **Fig. 8** shows

the wind at 850 hPa and sea level pressure causing atmospheric stability on the Southeast, especially over SP, on 23 and 24 October. This stability is caused by the high-pressure system acting over the Atlantic Ocean reaching 1030 hPa over the Atlantic Ocean. The synoptic conditions were associated with another low-pressure system of 998 hPa, over Bolivia and a high-pressure system of 1030 hPa over the south and southeast coast and remained there for these days. During October 23-24, the weather situation over the state of SP is calm and stable. In general, higher pollutant concentrations can be observed in the presence of the high-pressure system, with stagnation of air circulation and more stable atmospheric conditions. The low-pressure system further South-west is responsible for atmospheric disturbances on October 25 causing instability over SP state. According to data from the National Institute of Meteorology (INMET, 2016) it rained over the MASP on October 25.

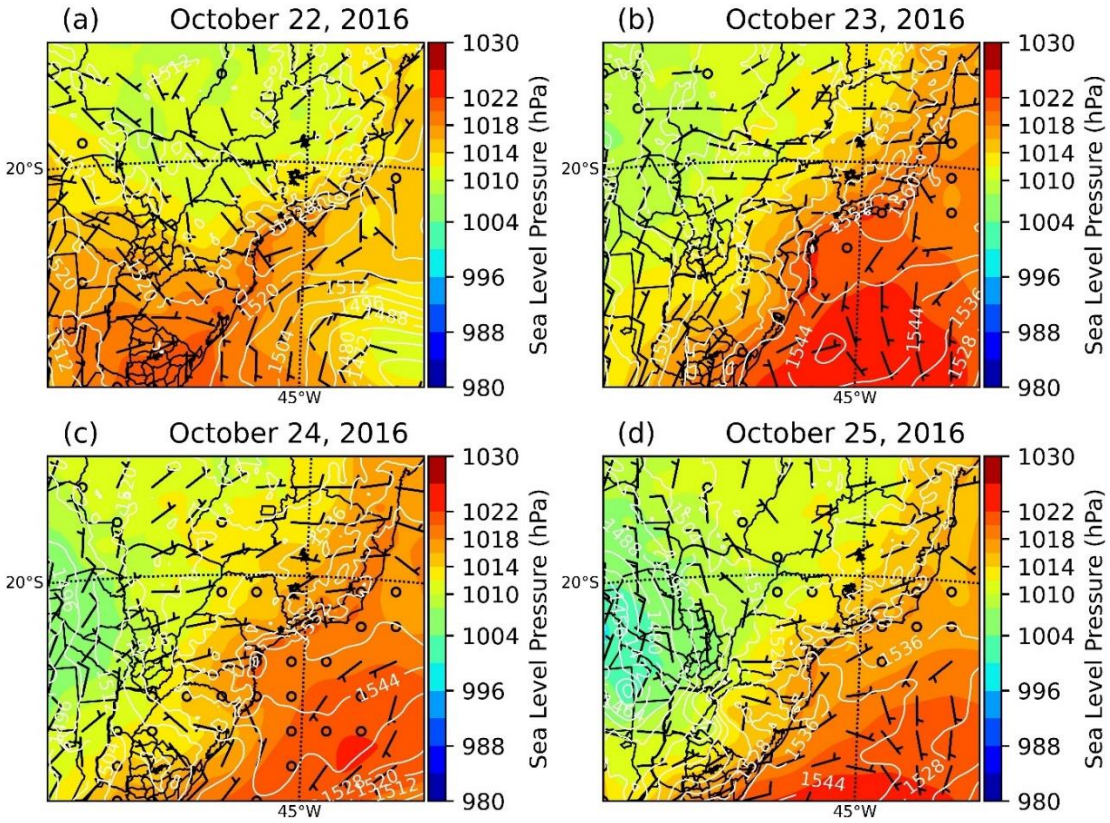

Fig. 8. Sea level pressure (hPa) (color code jet), wind (m/s) and geopotential height (m) at 850 hPa represented by the white lines simulated by WRF for October **(a)** 22, **(b)** 23, **(c)** 24 and **(d)** 25, 2016, with 25 km horizontal resolution**.**

Fig. 9 presents AOD (Levy et al., 2013; Sayer et al., 2017), MODIS fire hotspots and thermal anomalies from Terra (MOD14) and Aqua (MYD14) for October 24 and 25, 2016, and vertical aerosol backscatter coefficients for 355 nm and 532 nm profiles for October 24, 2016. On October 24 and 25 (**Fig. 9a** and **Fig. 9b)** the atmosphere was cloudy over the MASP. Between 10:30 and 11:30 LT, the backscatter profile retrieved by the SPU-Lidar station presents three different aerosol layers. The first one, with a backscatter peak of 0.004 $km^{-1}sr^{-1}$, is due to the aerosol particulate trapped inside the PBL. The second one is an aerosol layer detached from the PBL, with a strong and sharp peak of 0.003 $km^{-1}sr^{-1}$ at 1440 m a.g.l., which can be associated

with the intrusion of polluted air into MASP. The third aerosol layer detected is located between 2300 – 3700 m a.g.l. and also, due to the altitude range, can be associated to aerosol transported from long-range distances to MASP. For this case the total column Lidar ratio at 532 nm is 83 sr and can be associated to absorbing particles from biomass-burning (Weitkamp, 2005). The meteorological condition for October 24 shows stable atmospheric conditions which are favorable to pollutant accumulation. At 850 hPa the wind is coming from several direction reaching the MASP between October 22-25 (**Fig. 8**).

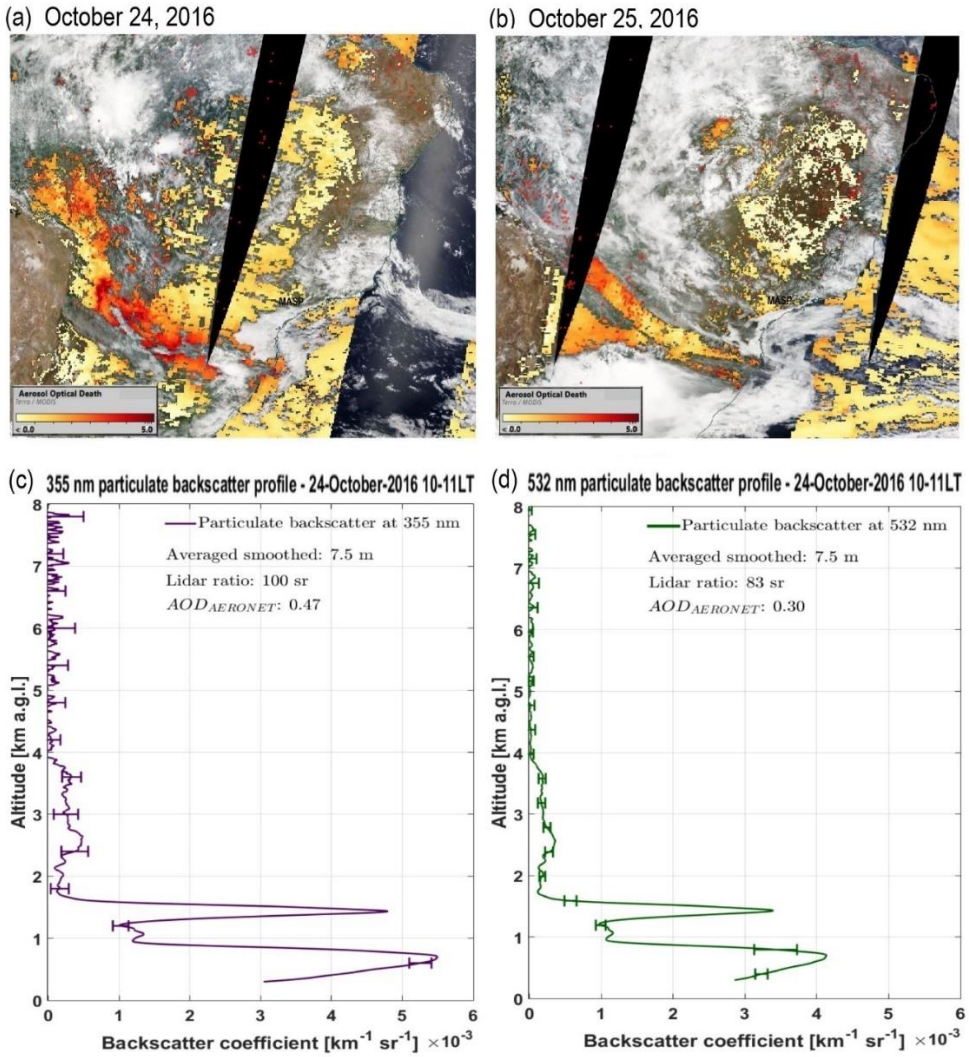

Fig. 9. AOD from Terra (MOD04_L2), Aqua (MYD04_L2), MODIS Fire hotspots and Thermal Anomalies product from Terra (MOD14), Aqua (MYD14) across Brazil and other South American countries **(a) on** October 24, 2016 and **(b)** on October 25, 2016 (Source: Nasa, 2020); the Backscatter backscatter profiles on October 24, 2016, between 10:30 and 11:30 LT from the IPEN Lidar in the MASP at: **(c)** 355 and **(d)** 532 nm.

Fig. 10 shows simulated PM2.5 concentrations at 850 hPa on a 5 km horizontal resolution on October 24 at 1800 and at 2200 LT (**Fig. 10a** and **10b**), as well as on October 25 at 0400 and 0800 LT (**Fig. 10c** and **10d**). These times were chosen because they best represent the PM2.5 transport at 850 hPa level (simulations of PM2.5 and PM10 for October 22, at 0400 LT to October 25, 1200 LT at 850 hPa for 1km resolution are shown in **Fig. S3** and **Fig. S4**). Especially on October 25, the pollution transported between MASP and MARJ

(429 km distance) via the Paraíba Valley is clearly visible. Concentrations of over 25 μg/m^3 are observed over the MASP on October 24 at 1800 LT and at 2200 LT at 850 hPa. This pollution is generated for the most part by evening rush hour and industries. Even with the high-pressure system affecting the atmospheric dynamics of the region (**Fig 8**) it is possible to see that pollution is transported between the MASP and MARJ not only through the coast via the sea-breeze, but also through the Paraíba Valley. EURAD-IM simulations show that pollutant transport in coastal regions such as S-Coast and MARJ are highly influenced by the dynamics of sea breezes and land breezes in these regions.

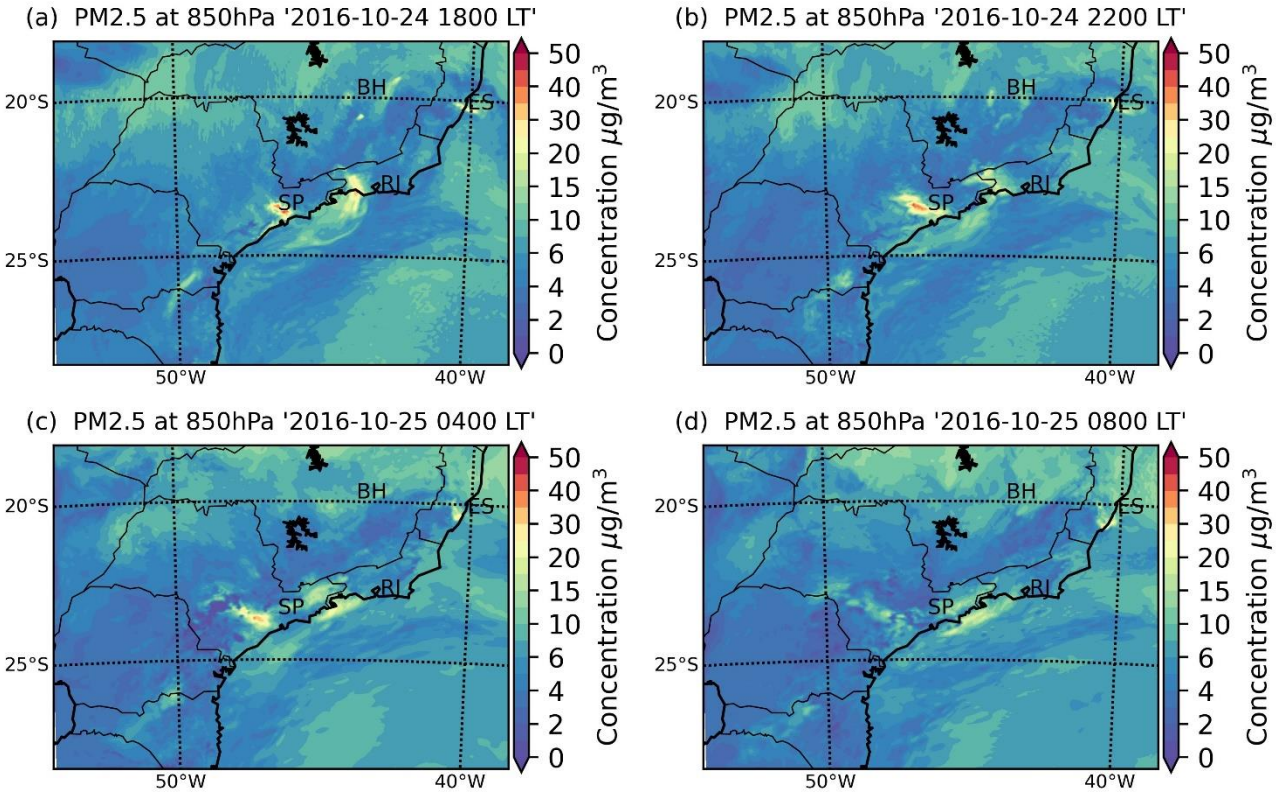

Fig. 10. EURAD-IM simulations with 5 km horizontal resolution at 850hPa: PM2.5 concentration at **(a)** 1800 LT on October 24, 2016; **(b)** 2200 LT on October 24, 2016; and **(c)** 0800 LT on October 25, 2016.

Fig. 11 shows the PM2.5 concentrations on the 1- km model domain at surface for October 24 at 1800 LT, and 2200LT, and for October 25 at 0800 LT. As expected, the high-resolution grid shows a higher PM concentration over the MASP mainly caused by vehicular emissions during the evening rush hours at around 1800 LT (**Fig. 11a**), as well as by industrial activities. **Fig. 11** also shows the transport of PM2.5 from MARJ to MASP with concentrations of over 20 μg/m^3 at 850 hPa on October 24, both at 1800 LT and 2200 LT via the coast, transported by the sea-breeze over the Atlantic and entering through the coast of Santos City into the direction of MASP. Also, a particle loaded air mass is coming through the Paraíba Valley from Rio de Janeiro in the direction of MASP. A similar behavior can be seen for PM10 (**Fig. S4**).

At 850 hPa, with predominant wind direction east-northeast at Paraíba Valley and the coastal region of Santos (**Fig 8c** and **Fig8d**), we faced the inverted situation than in the prior case study. For this reason, we calculated how much the PM10 and PM2.5 plumes at 850 hPa contributed to the total PM10 and PM2.5

concentration over MASP. We estimated that 26 % of the total PM10 and 28 % of the total PM2.5 at 850 hPa at MASP are coming from Vale do Paraíba in October 24-25, while Santos contributed with 24 % of the total PM10 and 34 % of the total PM2.5. These results together with the analyzed meteorological data, show that the air pollution plumes from MASP and MARJ interact with each other depending on the meteorological conditions via two possible routes: via the Paraíba Valley and via the Rio de Janeiro/São Paulo coast. Freitas et al., (2005) studied the meteorological conditions that favor these pollutants transport such as large-scale circulation in central-south-southeast region of Brazil, low- and high-pressure zones and local circulations such as sea breeze propagation, a factor that determines the dispersion of pollutants over MASP. Another important forcing is the complex topography of the region that can generate mountain-valley circulations mainly in the eastern and northwestern portions of MASP, between the Serra da Mantiqueira and the Paraíba Valley (Freitas et al., 2005). The Urban Heat Island (UHI) is another forcing that impact the local circulation and is provoked by the effect of urbanization and by human activities in MASP and MARJ.

The abrupt change in PM10 and PM2.5 concentrations between October 24 to 25 is due to late rain on October 24 in MASP, while in the MARJ the conditions remained dry according to meteorological data from the INMET (2016). **Fig. 11g** and **Fig. 11h** show PM2.5 concentrations for the lowest 10 levels of the model, showing the complex vertical structure of PM distribution. **Fig. 11g** shows a strong vertical mixing above MASP indicating the presence of an Urban Heat Island (UHI), a common meteorological phenomenon first studied over the MASP by Freitas et al. (2005), who concluded that the UHI forms a strong convergence zone in the center of the city and thereby accelerates the sea-breeze front toward the city center.

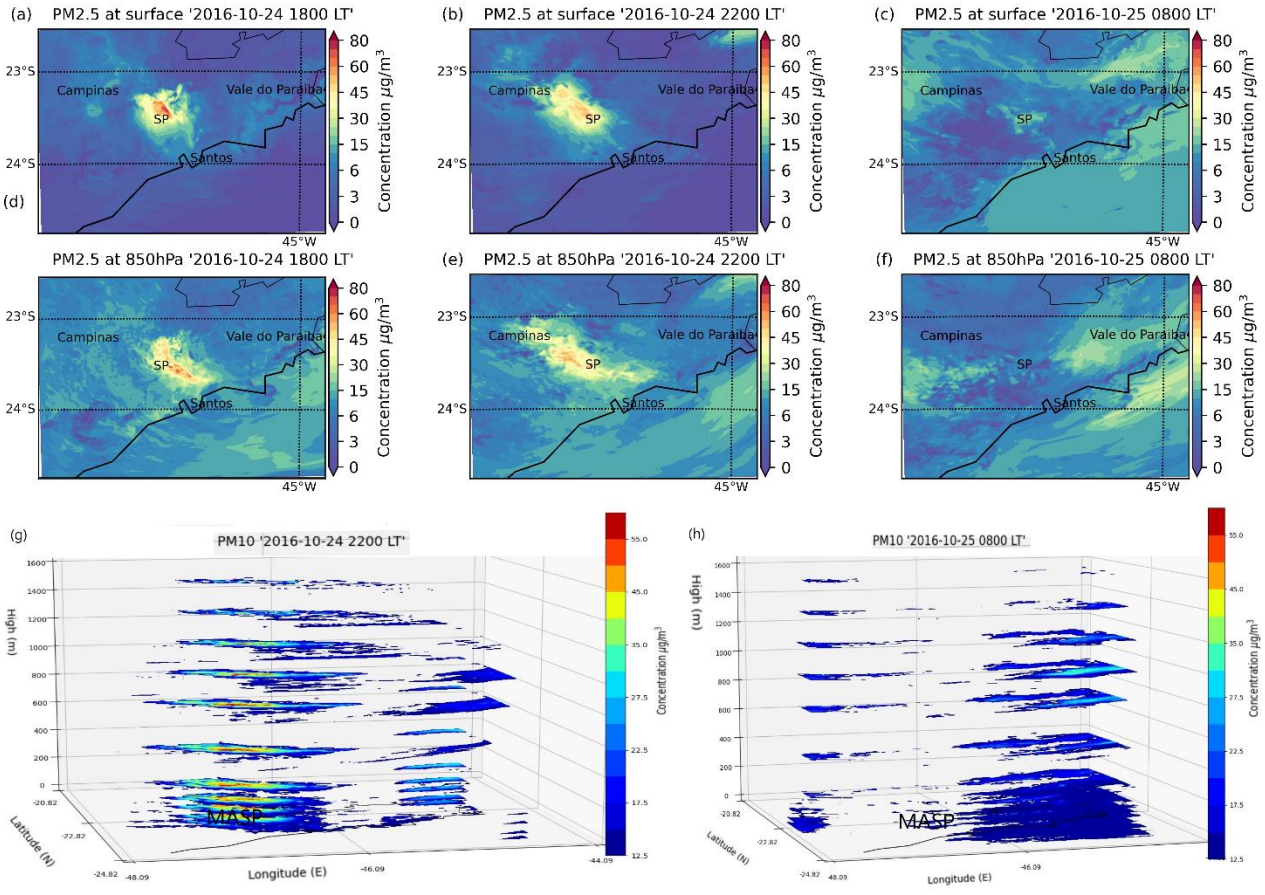

Fig. 11. PM2.5 concentration simulated by EURAD-IM on the 1-km domain at surface on October 24, 2016, 1800 LT (a); 2200 LT (b) and on October 25, 2016, 0800 LT (c). PM2.5 concentration simulated by EURAD-IM on the 1-km domain at 850 hPa on October 24, 2016, 1800 LT (d); 2200 LT (e) and on October 25, 2016, 0800 LT (f). PM2.5 concentrations on October 24, at 2200 LT **(g)** and October 25, at 0800 LT **(h),** 2016 for the lowest 10 levels of the model.

Fig. 12 compares the modeled and observed PM10 and PM2.5 times series for October 22-25 clustered according to **Table 1** (supplementary material) and **Table 5** presents statistical indexes for PM10 and PM2.5 for the October case study. For this second case study the datasets remain with the Pearson coefficient mostly varying between 0.50-0.70 for PM10, with the exception of NW PAULÍNIA with a correlation coefficient of 0.87, which constitutes a fairly strong positive relationship. Although the EURAD-IM simulation involves anthropogenic emissions, it is necessary to improve the emissions inventories to provide an as accurate as possible and consistent image of the atmosphere state at a given time. The vehicle, industrial and agricultural emissions scenario needs to be better defined for the region. The EURAD-IM performs well in MASP Center that contains more observational sites and thus more representative standard deviations could be calculated. Model and observations agree within the error range (**Fig. 12a**). For the clusters MASP CENTER, S-Coast, NW PAULÍNIA, NW CAMPINAS and NW LIMEIRA (**Fig 12a, Fig 12c-f)**, EURAD-IM simulations were inside the standard deviations of the observations with RMSE = 3.53 (**Table 5)**. EURAD underestimates concentrations at MASP CENTER, MASP North, NW PAULÍNIA, NW CAMPINAS, NW LIMEIRA, E-Vale do Paraíba and overestimate at S-Coast. For PM2.5 concentrations at MASP CENTER the model did not show a good performance with a Pearson coefficient of r = 0.35 overestimating the observations by 76 $\mu g/m^3$. The PM10 concentration for October 22-25 was lower than during July 10-13 possibly related to the transition seasons and onset of the wet season during this month. These results also show that EURAD-IM requires more concise emission estimates to quantitatively reproduce the atmospheric state. The quality of results obtained is directly related to the quality and detail of the underlying atmospheric emission inventory of the region. Regarding Brazil, only very few cities have detailed inventories, and the use of global inventories is thus often unavoidable. Also, EURAD-IM is a mesoscale-alpha regional model working on a maximum horizontal resolution of 1 km and therefore steep and abrupt changes in vertical surface structure, typical for urban environments, cannot be resolved.

Differences in concentrations can reach more than 95 $\mu g/m^3$: average concentrations of the C – MASP NORTH cluster on October 25 at 2100 LT were 118 $\mu g/m^3$, while the model's average E – MASP North reached only 21 $\mu g/m^3$. Other high PM10 concentrations occurred on October 22 at C - NW Paulínia cluster, reaching a maximum concentration of 105 $\mu g/m^3$, while the average model concentration at E – NW Paulínia was 44 $\mu g/m^3$.

Table 4

Model quality indicators calculated with hourly concentration observed/modeled on October 22-25, in 26 background sites (20 PM10 and 5 PM2.5 measurement sites) grouping in 8 clusters according to **Table 3**.

Cluster Name	r	RMSE	Bias
MASP Center (PM10)	0.75	3.53	-7.50
MASP North (PM10)	0.34	17.36	-8.70
NW Paulínia (PM10)	0.86	21.52	-41.90
NW Campinas (PM10)	0.61	7.40	-14.80
NW Limeira (PM10)	0.59	9.38	-17.20
S-Coast (PM10)	0.53	5.88	18.30
E-Vale do Paraíba (PM10)	0.60	7.21	-2.90
MASP (PM2.5)	0.35	9.47	76.40

678

679

680

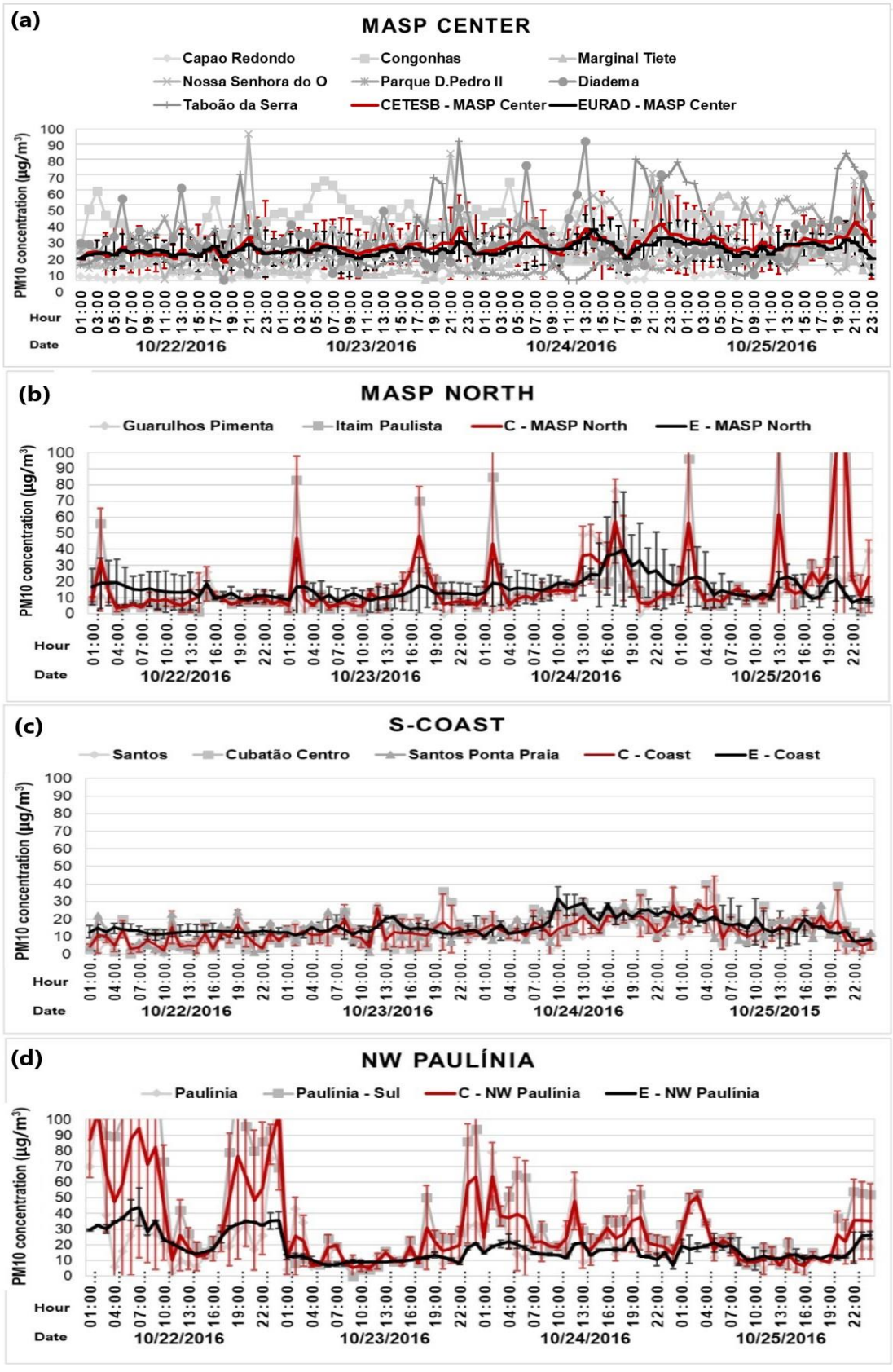

Fig. 12. PM10 concentrations for October 22-25, 2016 measured by CETESB stations and modelled by EURAD-IM. For each CETESB super-observation (red) the original data at the observation sites (grey) and EURAD-IM super-observation (black) are given. **Table 3** defines the cluster grouping.

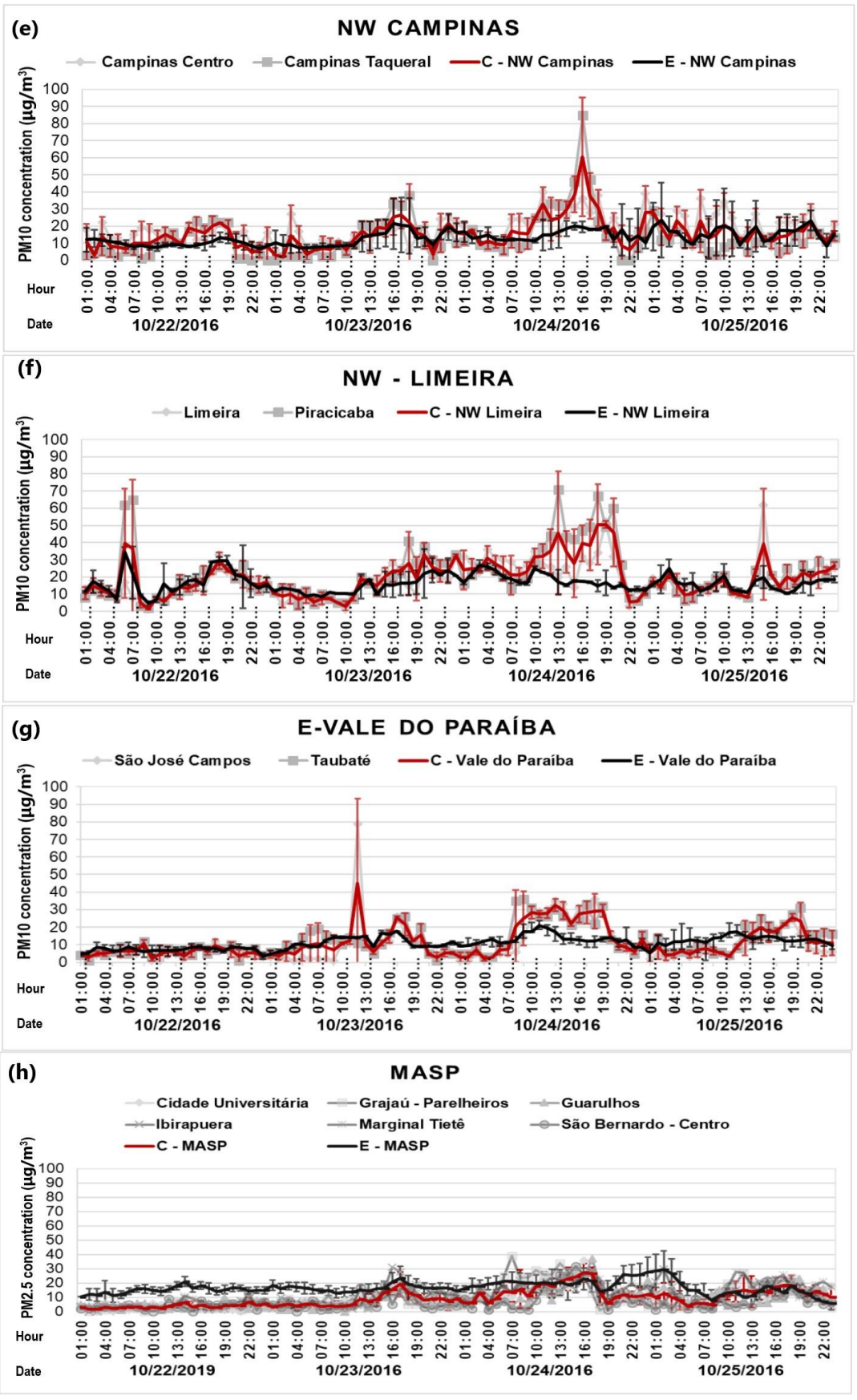

Fig. 12. Continued.

CONCLUSIONS

690
691 The mechanisms of elevated air pollution in the MASP have been studied by a novel modeling
692 approach, resting on (i) a multiscale and multi-resolution model configuration, encompassing the MASP by
693 a 25 km resolution domain over most part of South America, a 5 km domain over the Southeast Brazil and 1
694 km domain centered over the MASP and (ii) two weather situations prone to air quality decline. The first
695 case study was set during the dry season of July, 2016, one of the months marked by frequent annual episodes
696 of long-range and regional pollution transport. The EURAD-IM elucidates well the role of the SALLJ in this
697 long-range transport of PM from the center of South America and the local transport within SP state
698 deteriorating the air quality of MASP. This pollution reaches the MASP and is also transported from the
699 MASP following the northeastern direction through the Paraíba Valley and Atlantic coast, which is divided
700 by the *Serra do Mar* (sea mountains) to Rio de Janeiro. The model reproduces the behavior of observed PM10
701 concentrations but underestimated the observations, although it presents a Pearson coefficient $r > 0.7$ for the
702 cluster in MASP Center. The second case study occurred from October 22–25, 2016, which is the transition
703 season from dry winter to wet summer in southeastern Brazil. EURAD-IM simulations show that the air
704 pollution from MASP and MARJ interact with each other depending on the meteorological conditions via
705 two possible routes: via the Paraíba Valley or via the Rio de Janeiro/São Paulo coast. In both case studies,
706 EURAD-IM results demonstrated that there can be exchange of pollutants between MASP and MARJ. In
707 general, the model somewhat underestimates the observations which is explained by the scale of the model
708 (1 km domain, as highest resolution) and the representativity of surface local observations in a highly variable
709 chemical regime. These results also show that EURAD-IM requires better emissions inventories to reproduce
710 an atmospheric state closer to the real state, as the vehicular, industrial and agricultural emissions from
711 EDGAR do not represent well the PM2.5 emissions. The results and their limits clearly indicate that further
712 detailed analyses of air quality conditions of the state of SP would highly benefit from a denser observation
713 network, especially outside the city, which also measures fine particulate matter (PM2.5). As a next step,
714 sensitivity tests will be performed including a high-resolution vehicular emission inventory for MASP and
715 Brazil and make use of the 4D-Var assimilation system that is part of EURAD-IM to optimize the model
716 results by assimilating heterogeneous in-situ and remote sensing observational data.
717

718 **Acknowledgements**

719 We thank the *Rheinisches Institut für Umweltforschung an der Universität zu Köln*, Germany for their
720 continuous support and for hosting Ediclê Duarte during his 12 months research visit in 2018/2019, together
721 with Research Centre Jülich. The authors gratefully acknowledge the computing time granted through JARA
722 on the supercomputer JURECA at *Forschungszentrum Jülich*. This study was financed in part by the
723 *Coordenação de Aperfeiçoamento de Pessoal de Nível Superior - Brazil* (CAPES) - Finance Code 001, Brazil,
724 for the doctoral scholarship granted. São Paulo State Environmental Sanitation Technology Company
725 (CETESB, Environmental Protection Agency) for the PM data. This article and the research behind it are a
726 direct contribution to the research themes of the Klimapolis Laboratory (klimapolis.net). Networking and

coordination activities of the Klimapolis Laboratory are funded by the German Federal Ministry of Education and Research (BMBF).

References

Albuquerque T.T., Andrade M.F., Ynoue R.Y. (2012). Characterization of atmospheric aerosols in the city of São Paulo, Brazil: comparisons between polluted and unpolluted periods. Environmental Monitoring and Assessment, https://doi.org/10.1007/s10661-011-2013-y.

Albuquerque T.T.A., Andrade M.F., Ynoue, R.Y., Moreira, D.M., Andreão, W.L., Santos, F.S., Nascimento, E.G.S., (2018). WRF-SMOKE-CMAQ modeling system for air quality evaluation in São Paulo megacity with a 2008 experimental campaign data. Environmental Science and Pollution Research, https://doi.org/10.1007/s11356-018-3583-9.

Albuquerque, T.T.A., West, J., Andrade, M.F., Ynoue, R.Y., Andreão, W.L., Santos, F.S., Maciel, F.M., Pedruzzi, R., Mateus, V.O., Martins, J.A., Martins, L.D., Nascimento, E. G.S., Moreira, D.M. (2019). Analysis of PM2.5 concentrations under pollutant emission control strategies in the metropolitan area of São Paulo, Brazil. Environmental Science and Pollution Research, https://doi.org/10.1007/s11356-019-06447-6.

Allen, A.G., McGonigle, A.J.S., Cardoso, A.A., Machado, C.M.D., Davison, B., Paterlini, W.C., Rocha, G.O., Andrade, J.B., 2009. Influence of sources and meteorology on surface concentrations of gases and aerosols in a coastal industrial complex. J. Braz. Chem. Soc. 20, 214e221. http://dx.doi.org/10.1590/ S0103-50532009000200004.

Alonso, M.F., Longo, K., Freitas, S., Fonseca, R., Marécal, V., Pirre, M., Klenner, L. (2010). An urban emission inventory for South America and its application in numerical modeling of atmospheric chemical composition at local and regional scales. Atmospheric Environment, https://doi.org/10.1016/j.atmosenv.2010.09.013.

Ackermann, I. J. MADE: Entwicklung und Anwendung eines Aerosol-Dynamik modells für dreidimensionale Chemie-Transport-Simulationen in der Troposphäre, Ph.D. Thesis, Institutfür Geophysik und Meteorologie der Universität zu Köln, 1997.

Ansmann A., Muller D. (2005). Lidar and Atmospheric Aerosol Particles. In: Weitkamp CE Lidar: range-resolved optical remote sensing of the atmosphere. Springer Series in Optical sciences, vol 102, chap 4. Springer Science, Heidelberg, UK, pp 105–141.

Ackermann I. J., Hass H., Memmesheimer M., Ebel A., Binkowski F. S., Shankar U. (1998). Modal Aerosol Dynamics model for Europe: Development and first applications. Atmospheric Environment, 32, 2981–2999.

Andreão W.L., Albuquerque T.T.A., Kumar P. (2018). Excess deaths associated with fine particulate matter in Brazilian cities. Atmospheric Environment, https://doi.org/10.1016/j.atmosenv.2018.09.034.

Andreão W.L., Alonso M.F., Pinto J.A., Pedruzzi R., Albuquerque T.T.A. (2020). Top Down Vehicle Emission Inventory for spatial distribution and dispersion modeling of particulate matter. Environmental Science and Pollution Research, https://doi.org/10.1007/s11356-020-08476-y.

Arakawa A., Lamb V. R. Computational design for the basic dynamical processes of UCLA general circulation model. Journal of Computational Physics, http://dx.doi.org/10.1016/B978-0-12-460817-7.50009-4.

Asmi E., Matti A., Tarja Y., Matti J., Päivi A., Timo M., Risto H., Kaarle H. (2009). Driver and passenger exposure to aerosol particles in buses and trams in Helsinki, Finland. Science of The Total Environment, https://doi.org/10.1016/j.scitotenv.2009.01.004.

Andreão W. L., Pinto J. A., Pedruzzi R., Kumar P., Albuquerque T. T. A. (2020). Quantifying the impact of particle matter on mortality and hospitalizations in four Brazilian metropolitan areas. Journal of Environmental Management, https://doi.org/10.1016/j.jenvman.2020.110840.

Andrade M.F., Miranda R.M., Fornaro A., Kerr A., Oyama B., Andre P.A., Saldiva P. (2012). Vehicle emissions and PM2.5 mass concentrations in six Brazilian cities. Air Quality, Atmosphere & Health, https://doi.org/10.1007/s11869-010-0104-5.

776 Andrade M.F., Ynoue R.Y., Freitas E.D., Todesco E., Vara Vela A., Ibarra S., Martins L.D., Martins J.A.,
777 Carvalho V.S.B. (2015). Air quality forecasting system for southeastern Brazil. Frontiers in Environmental
778 Science, https://doi.org/10.3389/fenvs.2015.00009.
779 Andrade M.F., Kumar P., Freitas E.D., Ynoue R.Y., Martins J., Martins L.D., Nogueira T., Perez-Martinez P.,
780 Miranda R.M., Albuquerque T.T., Gonçalves F.L.T., Oyama B., Zhang Y. (2017). Air quality in the
781 megacity of São Paulo: evolution over the last 30 years and future perspectives. Atmospheric Environment,
782 https://doi.org/10.1016/j.atmosenv.2017.03.051.
783 Artaxo P., Fernandes E.T., Martins J. V., Yamasoe M. A., Hobbs, P.V., Maenhaut, W., Longo, K. M., Castanho
784 A., (1998). Large Scale Aerosol Source Apportionment in Amazonia. Journal of Geophysical Research,
785 103 (D24): 31.837-31.848.
786 Artaxo, P., Andreae, M.O., Guenther A., Rosenfeld D. (2001). LBA Atmospheric Chemistry: Unveiling the
787 lively interactions between the biosphere and the Amazonian atmosphere. In: IGBP Global Change
788 Newsletter, LBA Special Issue, 12-15.
789 Artaxo P.V.G., Gatti A.M.C., Leal K.M., Longo S.R., Freitas L.L., Lara T.M., Pauliquevis A.S., Procópio,
790 Rizzo L. V. (2005). Química atmosférica na Amazônia: A floresta e as emissões de queimadas
791 controlando a composição da atmosfera amazônica. Acta Amazon, doi:10.1590/S0044-59672005000200008.
792 Aleksankina K., Reis S., Vieno M., Heal M.R. (2019). Advanced methods for uncertainty assessment and
793 global sensitivity analysis of a Eulerian atmospheric chemistry transport model. Atmospheric Chemistry
794 and Physics, https://doi.org/10.5194/acp-19-2881-2019.
795 Alonso M.F., Longo K., Freitas S., Fonseca R., Marécal V., Pirre M., Klenner L. (2010) An urban emission
796 inventory for South America and its application in numerical modeling of atmospheric chemical
797 composition at local and regional scales. Atmospheric Environment,
798 https://doi.org/10.1016/j.atmosenv.2010.09.013.
799 Andreae, M.O., Merlet, P. (2001). Emission of trace gases and aerosols from biomass burning, global
800 biogeochemical cycles, https://doi.org/10.1029/2000GB001382.
801 Benedetti A., Morcrette J.J., Boucher O., Dethof A., Engelen R.J., Fisher M., Flentje H., Huneeus N., Jones
802 L., Kaiser J. W., Kinne S., Mangold A., Razinger M., Simmons A. J., Suttie M., and the GEMS-AER team.
803 (2009). Aerosol analysis and forecast in the European Centre for Medium-Range Weather Forecasts
804 Integrated Forecast System: Data Assimilation. Journal of Geophysical Research,
805 https://doi.org/10.1029/2008JD011115.
806 Baars H., Kanitz T., Engelmann R., Althausen D., Heese B., Komppula M., Preißler J., Tesche M., Ansmann
807 A., Wandinger U., Lim J.-H., Ahn J.Y., Stachlewska I.S., Amiridis V., Marinou E., Seifert P., Hofer J.,
808 Skupin A., Schneider F., Bohlmann S., Foth A., Bley S., Pfüller A., Giannakaki E., Lihavainen H., Viisanen
809 Y., Hooda R. K., Pereira S.N., Bortoli D., Wagner F., Mattis I., Janicka L., Markowicz K.M., Achtert P.,
810 Artaxo P., Pauliquevis T., Souza R. A. F., Sharma V. P., van Zyl P. G., Beukes J. P., Sun J., Rohwer E. G.,
811 Deng R., Mamouri R.E., Zamorano F. (2016). An overview of the first decade of PollyNET: an emerging
812 network of automated Raman-polarization lidars for continuous aerosol profiling. Atmospheric Chemistry
813 and Physics, https://doi.org/10.5194/acp16-5111-2016.
814 Binkowski F. S., U. Shankar (1995). The regional particulate matter model 1. Model description and
815 preliminary results. Journal of Geophysical Research, https://doi.org/10.1029/95JD02093.
816 Bahreini R., Ahmadov R., McKeen S., Vu K., Dingle J., Apel E. (2018). Sources and Characteristics of
817 Summertime Organic Aerosol in the Colorado Front Range: Perspective from Measurements and WRF-
818 Chem Modeling. Atmospheric Chemistry and Physics, http://dx.doi.org/10.5194/acp-2018-57.
819 Boldo E., Linares C., Aragonés N., Lumbreras J., Borge R., De La Paz D., Pérez- Goméz B., Fernández-
820 Navarro P., García-Pérez J., Pollán M., Ramis R., Moreno T., Karanasiou A., López-Abente G. (2014). Air
821 quality Modeling and mortality impact of fine particles reduction policies in Spain. Environmental
822 Research, https://doi.org/10.1016/j.envres.2013.10.009.
823 CETESB Relatório de Qualidade do ar no estado de São Paulo. (2016). Companhia Ambiental do Estado de
824 São Paulo (São Paulo State Environmental Protection Agency). http://ar.cetesb.sp.gov.br/publicacoes-
825 relatorios/ (accessed June 13, 2019).

826 CETESB Relatório de Qualidade do ar no estado de São Paulo. (2009). Companhia Ambiental do Estado de
827 São Paulo (São Paulo State Environmental Protection Agency). http://ar.cetesb.sp.gov.br/publicacoes-
828 relatorios/ (accessed June 13, 2019)
829 CETESB Relatório de Qualidade do ar no estado de São Paulo. (2017). Companhia Ambiental do Estado de
830 São Paulo (São Paulo State Environmental Protection Agency). http://ar.cetesb.sp.gov.br/publicacoes-
831 relatorios/ (accessed June 13, 2019)
832 Campbell P., Zhang Y., Yan F., Lu Z., Streets D. (2018). Impacts of transportation sector emissions on future
833 U.S. air quality in a changing climate. Part I: projected emissions, simulation design, and model evaluation.
834 Environmental Pollution, https://doi.org/10.1016/j.envpol.2018.04.020.
835 Carvalho V.S.B., Freitas E.D., Martins L.D., Martins J.A., Mazzoli C.R., Andrade M.F. (2015). Air quality
836 status and trends over the Metropolitan Area of São Paulo, Brazil as a result of emission control policies.
837 Environmental Science & Policy, doi:10.1016/j.envsci.2014.11.001.
838 Crippa M., Diego G., Marilena M., Edwin S, Frank D., John A.A., Suvi M., Ulrike D., Jos G. J.O., Valerio P.
839 (2018). Greet Janssens-Maenhout1 Gridded Emissions of Air Pollutants for the period 1970-2012 within
840 EDGAR v4.3.2. Earth System Science Data., https://doi.org/10.5194/essd-2018-31.
841 Collet S., Kidokoro T., Karamchandani P., Jung J., Shah T. (2018). Future year ozone source attribution
842 modeling study using CMAQ-ISAM. Journal of the Air & Waste Management Association,
843 https://doi.org/10.1080/10962247.2018.1496954.
844 Cotton W.R., Pielke S.R.A., Walko R.L., Liston G.E., Tremback C.J., Jiang H., Mcanelly R.L., Harrington J.
845 Y., Nicholls M.E., Carrio G.G., Mcfadden J.P. (2003). RAMS 2001: Current Status and Future Directions.
846 Meteorology and Atmospheric Physics, doi:10.1007/s00703-001-0584-9.
847 Capucim M.N., Brand V.S., Machado C.B., Martins L.D., Allasia D.G., Homann C.T., Freitas E.D., Silva D.,
848 Andrade M.F., Martins J.A. (2015). South America Land Use and Land Cover Assessment and Preliminary
849 Analysis of Their Impacts on Regional Atmospheric Modeling Studies. IEEE Journal of Selected Topics in
850 Applied Earth Observations and Remote Sensing, doi:10.1109/JSTARS.2014.2363368.
851 Damian-Iordache V. (1996). KPP - Chemistry Simulation Development Environment, Ph.D. Thesis, The
852 University of Iowa, Dezember, 1996.
853 de Oliveira, A.M., Mariano, G.L., Alonso, M.F. and Mariano, E.V.C. (2016b). Analysis of incoming biomass
854 burning aerosol plumes over southern Brazil. Atmos. Sci. Lett. 17: 577–585.
855 Dudhia J. (1989). Numerical study of convection observed during the Winter Monsoon Experiment using a
856 mesoscale two–dimensional model. Journal of the Atmospheric Sciences, doi:10.1175/1520-
857 0469(1989)046<3077:NSOCOD>2.0.CO;2PDF
858 Ding D., Zhu Y., Jang C., Lin C.-J., Wang S., Fu J., Gao J., Deng S., Xie J., Qiu X. (2016). Evaluation of health
859 benefit using BenMAP-CE with an integrated scheme of model and monitor data during Guangzhou Asian
860 Games. Journal of Environmental Sciences, https://doi.org/10.1016/j.jes.2015.06.003.
861 Ebel A., Elbern H., Feldmann H., Jakobs H.J., Kessler C., Memmesheimer M., Oberreuter A., Piekorz G.
862 (1997). Air pollution studies with the EURAD model system, vol 120, Mitteilungen aus dem Institut für
863 Geophysik und Meteorologie der Universität zu Köln, 1997.
864 Elbern H., H. Schmidt, Talagrand O., Ebel A. (2000). 4D-variational data assimilation with an adjoint air
865 quality model for emission analysis, Environmental Modelling & Software, https://doi.org/10.1016/S1364-
866 8152(00)00049-9.
867 Elbern H. and Schmidt H. (2002). Chemical 4D variational data assimilation and its numerical implications
868 for case study analyses, in IMA volumes in Mathematics and its Applications. Atmospheric Modeling,
869 https://doi.org/10.1007/978-3-642-12535-5_24.
870 Elbern H., Strunk A., Schmidt H. and Talagrand O. (2007) Emission rate and chemical state estimation by 4-
871 dimensional variational inversion. Atmospheric Chemistry and Physics, https://doi.org/10.5194/acp-7-
872 3749-2007.
873 Elbern H., Schwinger J., and Botchorishvili R. (2010). Chemical state estimation for the middle atmosphere
874 by four□dimensional variational data assimilation: System configuration. Journal of Geophysical
875 Research, doi:10.1029/2009JD011953.

Eurostat (2004) NAMEA for Air Emissions Compilation Guide, Luxembourg, Eurostat. [Google Scholar].

Fernald F.G. (1984). Analysis of atmospheric lidar observations: some comments. Applied Optics, https://doi.org/10.1364/AO.23.000652.

Flemming J., Huijnen V., Arteta J., Bechtold P., Beljaars A., Blechschmidt A.-M., Diamantakis M., Engelen R. J., Gaudel A., Inness A., Jones L., Josse B., Katragkou E., Marecal V., Peuch V.-H., Richter A., Schultz M. G., Stein O., and Tsikerdekis A. (2015). Tropospheric chemistry in the Integrated Forecasting System of ECMWF. Geoscientific Model Development, https://doi.org/10.5194/gmd-8-975-2015.

Faiz A., Weaver C.S., Walsh M.P. (1996). Air pollution from motor vehicles: standards and technologies for controlling emissions. Published: November 1996, ISBN: 978-0-8213-3444-7 https://doi.org/10.1596/0-8213-3444-1.

Freitas S.R., Longo K.M., Silva Dias M.A.F., Chatfield R., Silva Dias P., Artaxo P., Artaxo M.O., Grell G., Rodrigues L. F., Fazenda A., Panetta J. (2009). The Coupled Aerosol and Tracer Transport model to the Brazilian developments on the Regional Atmospheric Modeling System (CATT-BRAMS) – Part 1: Model description and evaluation. Atmospheric Chemistry and Physics, https://doi.org/10.5194/acp-9-2843-2009.

Freitas, S.R., Longo, K.M., Silva Dias, M.A.F., Silva Dias, P.L., Chatfield, R., Prins, E. and Recuero, F.S. (2005). Monitoring the transport of biomass burning emissions in South America. Environ. Fluid Mech. 5: 135–167.

Freitas E.D., Rozoff C.M., Cotton W.R., Silva Dias P.L. (2007). Interactions of an urban heat island and sea breeze circulations during winter over the Metropolitan Area of São Paulo - Brazil. Boundary Layer Meteorology, doi: 10.1007/s10546-006-9091-3.

Freitas E.D., Martins L.D., Mazzoli C.R., Martins J. A., Hallak R., Itimura M.S., Carvalho V.S. B., Silva Dias P.L., Andrade M.F. (2007). Particulate Matter concentration forecast over the Metropolitan Area of São Paulo. Ciência e Natura, https://doi.org/10.5902/2179460X9914.

Freitas S.R., Longo K.M., Chatfield R., Latham D., Silva Dias M. A.F., Andreae M.O. Andreae, Prins E., Santos J. C., Gielow R., and Carvalho J.J.A.. (2007a). Including the sub-grid scale plume rise of vegetation fires in low resolution atmospheric transport models, Atmospheric Chemistry and Physics, https://doi.org/10.5194/acp-7-3385-2007.

Freitas S. R., Longo K. M., Silva Dias M. A. F., Chatfield R., Silva Dias P., Artaxo P., Andreae M. O., Grell, G., Rodrigues L. F., Fazenda A., and Panetta J. (2009). The Coupled Aerosol and Tracer Transport model to the Brazilian developments on the Regional Atmospheric Modeling System (CATT-BRAMS) – Part 1: Model description and evaluation, Atmospheric Chemistry and Physics, 9, 2843–2861, https://doi.org/10.5194/acp-9-2843-2009.

Freitas S.R., Panetta J., Longo k.M., Rodrigues L.F., Moreira DS., Rosario N.E., Silva Dias P.L., Silva Dias M.A.F., Souza E.P., Freitas E.D., Longo M., Frassoni A., Fazenda A.L., Santos E Silva C.M., Pavani C.A.B., Eiras D., Franca D.A., Massaru D., Silva F.B., Santos F.C., Pereira G., Camponogara G., Ferrada GA., Campos H.F., Campos V.H.F., Menezes I., Freire J.L., Alonso M.F., Gacita M.S., Zarzur M., Fonseca R.M., Lima R.S., Siqueira R.A., Braz R., Tomita S., Oliveira V., Martins L.D. (2017). The Brazilian developments on the Regional Atmospheric Modeling System (BRAMS 5.2): an integrated environmental model tuned for tropical areas. Geoscientific Model Development, http://dx.doi.org/10.5194/gmd-10-189-2017.

Jülich Supercomputing Centre. (2018). JURECA: Modular supercomputer at Jülich Supercomputing Centre. Journal of large-scale research facilities, 4, A132, http://dx.doi.org/10.17815/jlsrf-4-121-1.

Gama C., Ribeiro I., Lange A.C., Vogel A., Ascenso A., Seixas V., Elbern H., Borrego H., Friese E., Monteiro A. (2019). Performance assessment of CHIMERE and EURAD-IM' dust modules. Atmospheric Pollution Research, https://doi.org/10.1016/j.apr.2019.03.005

Guerrero-Rascado J. L., Landulfo E., Antuña J. C., Barbosa H. M. J., Barja B., Bastidas A. E., Bedoya A. E., da Costa R. F., Estevan R., Forno R. N., Gouveia D. A., Jimenez C., Larroza E. G., Lopes F. J. S., Montilla-Rosero E., Moreira G. A., Nakaema W. M., Nisperuza D., Alegria D., Múnera M., Otero L., Papandrea S.,

Pawelko E., Quel E.J., Ristori P., Rodrigues P. F., Salvador J., Sánchez M. F., and Silva A. (2014). Towards an instrumental harmonization in the framework of LALINET: dataset of technical specifications, Proc. SPIE 9246, Lidar Technologies, Techniques, and Measurements for Atmospheric Remote Sensing X, 92460O, doi:10.1117/12.2066873.

Guerrero-Rascado J.L., Landulfo E., Antuña, J. C., Barbosa H. M. J., Barja B, Bastidas A. E., Bedoya A. E., da Costa R. F., Estevan R., Forno R. N., Gouveia D. A., Jimenez C., Larroza E. G., Lopes F. J. S., Montilla-Rosero E., Moreira G. A., Nakaema W. M., Nisperuza D., Alegria D., Múnera M., Otero L., Papandrea S., Pawelko E., Quel E. J., Ristori P., Rodrigues P. F., Salvador J., Sánchez M. F., and Silva A. (2016). Latin American Lidar Network (LALINET) for aerossol research: Diagnosis on network instrumentation, Journal of Atmospheric and Solar-Terrestrial Physics, doi:10.1016/j.jastp.2016.01.001.

Granier C., Bessagnet B., Bond T., D'Angiola A., Denier van der Gon H., Frost G., Heil A., KaiserJ., Kinne S., Klimont Z., Kloster S., Lamarque J.-F., Liousse C., Masui T., Meleux F., Mieville A., Ohara T., Raut J.-C., Riahi K., Schultz M., Smith S., Thompson A., Aardenne J., Werf G., and Vuuren D. (2011). Evolution of anthropogenic and biomass burning emissions of air pollutants at global and regional scales during the 1980–2010 period. Climatic Change, doi:10.1007/s10584-011-0154-1.

Gurjar B.R., Butler T.M., Lawrence M.G. and Lelieveld, J. (2008). Evaluation of emissions and air quality in megacities. Atmospheric Environment. https://doi.org/10.1016/j.atmosenv.2007.10.048.

Gulia S., Shiva Nagendra S.M., Mukesh Khare, Isha Khanna. (2015). Urban air quality management-A review. Atmospheric Pollution Research, https://doi.org/10.5094/APR.2015.033.

Grell G.A., Peckham S.E., Schmitz R., McKeen S.A., Frost G., Skamarock W.C. (2005). Fully coupled "online" chemistry within the WRF model. Atmospheric Environment, doi: 10.1016/j.atmosenv.2005.04.027.

Grell G.A., and Freitas S.R. (2014). A scale and aerosol aware stochastic convective parameterization for weather and air quality modeling. Atmospheric Chemistry and Physics, 14, 5233-5250, doi:10.5194/acp-14-5233-2014.

Geiger H., I. Barnes I., Bejan T., Benter and Spittler M. (2003). The tropospheric degradation of isoprene: an updated module for the regional atmospheric chemistry mechanism. Atmospheric Environment, https://doi.org/10.1016/S1352-2310(02)01047-6.

Hart, W. and Spinfaiiae, J. (1999). Correlation between smoke and tropospheric ozone concentration in Cuiabá during Smoke. Clouds, and Radiation-Brazil (SCAR-B). J. Geophys. Res. 104: 12113–12129.

Hoelzemann J.J., Longo K.M., Fonseca R.M., Rosário N.M. E., Elbern H., Freitas S.R. (2009). Regional representativity of AERONET observation sites in South America determined by correlation studies with MODIS Aerosol Optical Depth. Journal of Geophysical Research: Atmospheres, https://doi.org/10.1029/2008JD010369.

Hong S.-Y., Yign N., Dudhia J. (2006). A new vertical diffusion package with an explicit treatment of entrainment processes. Monthly Weather Review, doi:10.1175/MWR3199.1.

Hong S.Y, Dudhia J., and Chen S.H. (2004). A revised approach to ice microphysical processes for the bulk parameterization of clouds and precipitation. Monthly Weather Review, doi:10.1175/1520-0493(2004)132<0103:ARATIM>2.0.CO;2.

Hass H. (1991). Description of the EURAD Chemistry–Transport–Model Version 2 (CTM2), vol 83, Mitteilungen aus dem Institut für Geophysik und Meteorologie der Universität zu Köln, 1991.

Hsu N. C., Hsu J., Sayer A. M., Kim W., Bettenhausen C., Tsay S.□C. (2019). VIIRS Deep Blue Aerosol Products Over Land: Extending the EOS Long□Term Aerosol Data Records. https://doi.org/10.1029/2018JD029688

Hsu N. C., Jeong M.-J., Bettenhausen C., Sayer A. M., Hansell R., Hansell C. S., Huang J., and Tsay S.-C. (2013). Enhanced Deep Blue aerosol retrieval algorithm: The second generation, J. Geophys. Res. Atmos., 118, 9296–9315, doi:10.1002/jgrd.50712.

971 Hollingsworth A., Engelen R. J., Textor C., Benedetti A., Boucher O., Chevallier F., Dethof A., Elbern H.,
972 Eskes H., Flemming J., Granier C., Kaiser J. W., Morcrette J.J., Rayner R., Peuch V.-H., Rouil L., Schultz
973 M. G., Simmons A. J., and The GEMS Consortium. (2008). Toward a Monitoring and Forecasting System
974 for Atmospheric Composition: The GEMS Project, Bulletin of the American Meteorological Society,
975 https://doi.org/10.1175/2008BAMS2355.1.
976 Huijnen V., Williams J., van Weele M., van Noije T., Krol M., Dentener F., Segers A., Houweling S., Peters
977 W., de Laat J., Boersma F., Bergamaschi P., van Velthoven P., Le Sager P., Eskes H., Alkemade F., Scheele
978 R., Nédélec P., and Pätz H.-W. (2010). The global chemistry transport model TM5: description and
979 evaluation of the tropospheric chemistry version 3.0. Geoscientific Model Development, doi:10.5194/gmd-
980 3-445-2010.
981 Hoesly R.M., Smith S. J., Feng L., Klimont Z., Janssens-Maenhout G., Pitkanen T., Seibert J. J., Vu, L., Andres
982 R. J., Bolt R. M., Bond T. C., Dawidowski L., Kholod N., Kurokawa J. I., Li M., Liu L., Lu Z., Moura
983 M.C.P., O'Rourke P.R., and Zhang Q. (2017). Historical (1750–2014) anthropogenic emissions of reactive
984 gases and aerosols from the Community Emission Data System (CEDS), Geoscientific Model
985 Development, doi:10.5194/gmd-2017-43.
986 Ibarra-Espinosa S., Ynoue R., O'Sullivan S., Pebesma E., Andrade M.D.F., Osses M. (2018). Vein v0.2.2: an
987 r package for bottom–up vehicular emissions inventories. Geoscientific Model Development,
988 https://doi.org/10.5194/gmd-11- 2209-2018.
989 IBGE. Diretoria de Pesquisas, Coordenação de População e Indicadores Sociais. 2018 e 2019 :estimativas das
990 populações residentes municipais calculadas com base na Projeção da população para o Brasil e Unidades
991 da Federação, por sexo e idade, Revisão 2018. Notas metodológicas podem ser consultadas em:
992 https://www.ibge.gov.br/estatisticas/sociais/populacao/9103-
993 estimativasdepopulacao.html?=&t=notastecnicas. Accessed July 01, 2020.
994 IBGE (2020). Available at: https://mapas.ibge.gov.br/fisicos/estaduais. Access on: May 17, 2020.
995 INPE, 2016. http://queimadas.dgi.inpe.br/queimadas/portal. Accessed July 01, 2020.
996 INMET, 2016. http://www.inmet.gov.br/portal/. Accessed May 15, 2019.
997 Inness, A., Ades, M., Agustí-Panareda, A., Barré, J., Benedictow, A., Blechschmidt, A.-M., Dominguez, J. J.,
998 Engelen, R., Eskes, H., Flemming, J., Huijnen, V., Jones, L., Kipling, Z., Massart, S., Parrington, M., Peuch,
999 V.-H., Razinger, M., Remy, S., Schulz, M., and Suttie, M.: The CAMS reanalysis of atmospheric
1000 composition, Atmos. Chem. Phys., 19, 3515–3556, https://doi.org/10.5194/acp-19-3515-2019, 2019.
1001 Janssens-Maenhout G., Crippa M., Guizzardi D., Dentener F., Muntean M., Pouliot G., Keating T., Zhang Q.,
1002 Kurokawa J., Wankmüller R., Denier van der Gon H., Kuenen J. J. P., Klimont Z., Frost G., Darras S., Koffi
1003 B., and Li M. (2015). HTAP_v2.2: a mosaic of regional and global e mission grid maps for 2008 and 2010
1004 to study hemispheric transport of air pollution. Atmospheric Chemistry and Physics, doi:10.5194/acp-15-
1005 11411-2015.
1006 Jiang N., Scorgie Y., Hart M., Riley M.L., Crawford J., Beggs P.J., Edwards G.C., Chang L., Salter D., Virgilio
1007 G.D. (2017). Visualizing the relationships between synoptic circulation type and air quality in Sydney, a
1008 subtropical coastal-basin environment. International Journal of Climatology,
1009 https://doi.org/10.1002/joc.4770.
1010 Jiang F., Liu Q., Huang X., Wang T., Zhuang B., Xie M. (2012). Regional modeling of secondary organic
1011 aerosol over China using WRF/Chem. Journal of Aerosol Science,
1012 https://doi.org/10.1016/j.jaerosci.2011.09.003.
1013 Kaiser J.W., Heil A., Andreae M.O., Benedetti A., Chubarova N., Jones L., Morcrette J.-J., Razinger M.,
1014 Schultz M.G., Suttie M., and van der Werf G.R. (2012). Biomass burning emissions estimated with a global
1015 fire assimilation system based on observed fire radiative power. Biogeosciences, doi:10.5194/bg-9-527-
1016 2012.

Klimont Z., Kupiainen K., Heyes C., Purohit P., Cofala J., Rafaj P., Borken-Kleefeld J., and Schöpp W. (2017). Global anthropogenic emissions of particulate matter including black carbon. Atmospheric Chemistry and Physics, https://doi.org/10.5194/acp-17-8681-2017.

Kumar P., Andrade M.F.A., Ynoue R.Y., Fornaro A., Freitas E.D., Martins J., Martins L.D., Albuquerque T.T., Zhang Y., Morawska L. (2016). New directions: From biofuels to wood stoves: The modern and ancient air quality challenges in the megacity of São Paulo. Atmospheric Environment doi: 10.1016/j.atmosenv.2016.05.059

Klett, J. D. (1983). Lidar calibration and extinction coefficients. Applied Optics, https://doi.org/10.1364/AO.22.000514, 1983.

Klett J.D. (1985). Lidar inversion with variable backscatter/extinction ratios, Applied Optics, https://doi.org/10.1364/AO.24.001638, 1985.

Longo K.M., Freitas S.R., Andreae M.O., Setzer A., Prins E., and Artaxo P. (2010). The Coupled Aerosol and Tracer Transport model to the Brazilian developments on the Regional Atmospheric Modeling System (CATT–BRAMS) – Part 2: Model sensitivity to the biomass burning inventories, Atmospheric Chemistry and Physics, 10, 5785–5795, doi:10.5194/acp-10-5785-2010.

Levy R. C., Mattoo S., Munchak L. A., Remer L. A., Sayer A. M., Patadia F., and Hsu N. C. (2013). The Collection 6 MODIS aerosol products over land and ocean. Atmospheric Measurement Techniques, https://doi.org/10.5194/amt-6-2989-2013.

Li J., Zhu Y., Kelly J.T., Jang C.J., Wang S., Hanna A., Xing J., Lin C.-J., Long S., Yu L. (2019). Health benefit assessment of PM2.5 reduction in Pearl River Delta region of China using a model-monitor data fusion approach. Journal of Environmental Management, https://doi.org/10.1016/j.jenvman.2018.12.060.

Lin L., Lee M.L., Eatough D.J. (2010). Review of recent advances in detection of organic markers in fine particulate matter and their use for source apportionment. Journal of the Air & Waste Management Association, doi:10.3155/1047-3289.60.1.3.

Libonati, R.; DaCamara, C.C.; Setzer, A.W.; Morelli, F.; Melchiori, A.E. (2015). An Algorithm for Burned Area Detection in the Brazilian Cerrado Using 4 μm MODIS Imagery. Remote Sensing, https://doi.org/10.3390/rs71115782.

Lanki T., Vanninen E., de Hartog J. *et al.* Effects of ultrafine and fine particulate and gaseous air pollution on cardiac autonomic control in subjects with coronary artery disease: The ULTRA study. Journal of Exposure Science & Environmental Epidemiology 16, 332–341 (2006). https://doi.org/10.1038/sj.jea.7500460.

Lopes F. J. S., Luis Guerrero-Rascado J., Benavent-Oltra J. A., Román R., Moreira G. A., Marques M. T. A., da Silva J. J., Alados-Arboledas L., Artaxo P., and Lan-dulfo E. (2018). Rehearsal for Assessment of atmospheric optical Properties during biomass burning Events and Long-range transportation episodes at Metropolitan Area of São Paulo-Brazil (RAPEL), EPJ Web of Conferences, https://doi.org/10.1051/epjconf/201817608011.

Lowe D., Archer-Nicholls S., Morgan W., Allan J., Allan S., Ouyang B., Le Breton E. M., Le Breton R. A., Di Carlo P., Percival C., Coe H., Jones R., and Jones G. (2015). WRF-Chem model predictions of the regional impacts of N2O5 heterogeneous processes on night-time chemistry over north-western Europe. Atmospheric Chemistry and Physics, doi:10.5194/acp-15-1385-2015.

Marécal V., Peuch V.-H., Andersson C., Andersson S., Arteta J., Beekmann M., Benedictow A., Bergström R., Bessagnet B., Cansado A., Chéroux F., Colette A., Coman A., Curier R. L., Denier van der Gon H. A. C., Drouin A., Elbern H., Emili E., Engelen R. J., Eskes H. J., Foret G., Friese E., Gauss M., Giannaros C., Guth J., Joly M., Jaumouillé E., Josse B., Kadygrov N., Kaiser J. W., Krajsek K., Kuenen J., Kumar U., Liora N., Lopez E., Malherbe L., Martinez I., Melas D., Meleux F., Menut L., Moinat P., Morales T., Parmentier J., Piacentini A., Plu M., Poupkou A., Queguiner S., Robertson L., Rouïl L., Schaap M., Segers A., Sofiev M., Tarasson L., Thomas M., Timmermans R., Valdebenito Á., van Velthoven P., van Versendaal R., Vira J., and Ung A. (2015). A regional air quality forecasting system over Europe: the MACC-II daily ensemble production. Geoscientific Model Development, https://doi.org/10.5194/gmd-8-2777-2015, 2015.

Masson V. (2000). A Physically-Based Scheme for the Urban Energy Budget in Atmospheric Models. Boundary-Layer Meteorology, doi:10.1023/A:1002463829265.

Memmesheimer M., Tippke J., Ebel A., Hass H., Jakobs H. J. and Jakobs M. (1991). On the use of EMEP emission inventories for European scale air pollution modelling with the EURAD model, in Proceedings of the EMEP workshop on photooxidant modelling for long range transport in relation to abatement strategies. https://doi.org/10.1007/978-3-662-03470-5_2.

Memmesheimer M., Jakobs H. J., Feldmann H., Feldmann G., Feldmann C., Feldmann E. and Ebel A. (2000). Computergestu¨tzte Langzeitsimulationen zur Bewertung von Strategien zur Luftreinhaltung, Abschlussbericht zum Vorhaben COSIMA im Auftrag des Landesumweltamtes Nordrhein-Westfalen.

Memmesheimer M., Friese E., Friese A., Friese H. J., Friese H., Kessler C., and Piekorz G. (2004). Long-term simulations of particulate matter in Europe on di erent scales using sequential nesting of a regional model. International Journal of Environment and Pollution, DOI: 10.1504/IJEP.2004.005530.

McRae G. J., W. R. Goodin and J. H. Seinfeld, Numerical solution of the atmospheric diffusion equation for chemically reacting flows. Journal of Computational Physics, https://doi.org/10.1016/0021-9991(82)90101-2.

Miranda R.M., Andrade M.F., Fornaro A., Astolfo R., Andre P.A., Saldiva P. (2012). Urban air pollution: a representative survey of PM2.5 mass concentrations in six Brazilian cities. Air Quality, Atmosphere & Health, https://doi.org/10.1007/s11869-010-0124-1.

Miranda R.M., Lopes F., Rosário N.É., Yamasoe M.A., Landulfo E., Andrade M.F. (2017). The relationship between aerosol particles chemical composition and optical properties to identify the biomass burning contribution to fine particles concentration: a case study for São Paulo city, Brazil. Environmental Monitoring & Assessment, https://doi.org/10.1007/s10661-016-5659-7.

Monahan, E. C., Coverage as a Remotely Monitorable Indication of the Rate of Bobbie Injection into the Oceanic Mixed Layer, Springer Netherlands, 1988.

Monteiro A., Ribeiro I., Tchepel O., Sá E., Ferreira J., Carvalho A., Martins V., Strunk A., Galmarini S., Elbern H., Schaap M., Builtjes P., Miranda A. I., and Borrego C. (2013). Bias Correction Techniques to Improve Air Quality Ensemble Predictions: Focus on O3 and PM Over Portugal. Environmental Modeling & Assessment, doi:10.1007/s10666-013-9358-2, 2013.

Morcrette J.-J., Boucher O., Jones L., Salmond D., Bechtold P., Beljaars A., Benedetti A., Bonet A., Kaiser J. W., Razinger M., Schulz M., Serrar S., Simmons A.J., Sofiev M., Suttie M., Tompkins A. M., and Untch A. (2009). Aerosol analysis and forecast intheEuropeanCentreforMedium-RangeWeatherForecastsIntegrated Forecast System: Forward modeling. Journal of Geophysical Research, https://doi.org/10.1029/2008JD011235, 2009.

Moreira D.S., Freitas S.R., Bonatti J.P., Mercado L.M., Rosario N.M.E., Longo K.M., Miller J.B., Gloor M., and Gatti L.V. (2013). Coupling between the JULES land-surface scheme and the CCATT–BRAMS atmospheric chemistry model (JULES-CCATT–BRAMS1.0): applications to numerical weather forecasting and the CO2 budget in South America. Geoscientific Model Development Discussions, doi:10.5194/gmdd-6-453-2013, 2013.

Mlawer E.J., Taubman S. J., Brown P.D., Iacono M. J., and Clough S.A. (1997). Radiative transfer for inhomogeneous atmospheres: RRTM, a validated correlated–k model for the longwave. Journal of Geophysical Research, doi:10.1029/97JD00237.

Molina L.T. *and* Molina M.J. (2002). Air Quality in the Mexico Megacity: An integrated Assessment; Kluwer Academic Publishers, Dordrecht, The Netherlands, 384p.

Molina L. T., Kolb C. E., de Foy B., Lamb B. K., Brune W. H., Jimenez J. L., Ramos-Villegas R., Sarmiento J., Paramo F.V. H., Cardenas B., Gutierrez-Avedoy V., and Molina M. J. (2007). Air quality in North America's most populous city – overview of the MCMA-2003 campaign. Atmospheric Chemistry and Physics, doi:10.5194/acp-7-2447-2007.

Molina M.J. & Molina L.T. (2004). Megacities and Atmospheric Pollution. Journal of the Air & Waste

Management Association, doi:10.1080/10473289.2004.10470936

Martins, L.D; Hallak, R.; Alves, R.C.; DE Almeida, D.S.; Squizzato, R.; Moreira, C.A.B.; Beal, A.; DA Silva, I; Rudke, A.; Martins, J. A. Long-Range Transport of Aerosols from Biomass Burning over Southeastern of South America and their Implications on Air Quality. Aerosol and Air Quality Research, v. 18, p. 1734, 2018. https://doi.org/10.4209/aaqr.2017.11.0545

Marengo J. A., Soares W. R., Saulo C., and Nicolini M. (2004). Climatology of the Low-Level Jet East of the Andes as Derived from the NCEP–NCAR Reanalyses: Characteristics and Temporal Variability. Journal of Climate, https://doi.org/10.1175/1520-0442(2004)017<2261:COTLJE>2.0.CO;2.

Müller D., Ansmann A., Mattis I., Tesche M., Wandinger U., Althausen D., & Pisani G. (2007). Aerosol-type-dependent lidar ratios observed with Raman lidar. Journal of Geophysical Research, doi: 10.1029/2006JD008292.

Nickovic, S., G. Kallos, A. Papadopoulos and O. Kakaliagou, A models for prediction of desert dust cycle in the atmosphere, Master Thesis, Journal of Geophysical Research, 2001.

Nogueira EM, Yanai AM, Fonseca FOR, Fearnside PM (2015) Carbon stock loss from deforestation through 2013 in Brazilian Amazonia. Global Change Biol 21(3):1271–1292. doi:10.1111/gcb.12798

NASA (National Aeronautics and Space Administration), source: https://worldview.earthdata.nasa.gov/ for July 11 and 12, respectively. Access on: June 13, 2020.

Rodrigues J.A., Libonati R., Pereira A.A., Nogueira J.M.P., Santos F.L.M., Peres L.F., Rosa A.S., Schroeder W., Pereira J.M.C., Giglio L., Trigo I.F., Setzer A.W. (2019). How well do global burned area products represent fire patterns in the Brazilian Savannas biome? An accuracy assessment of the MCD64 collections. International Journal of Applied Earth Observation and Geoinformation, https://doi.org/10.1016/j.jag.2019.02.010.

Pielke R. A., Cotton W. R., Walko L. R., Tremback C. J., Lyons W. A., Grasso L. D., Nicholls M. E., Moran M. D., Wesley D. A., Lee T. J., Copeland, J. H. (1992). A Comprehensive Meteorological Modeling System – RAMS, Meteorology and Atmospheric Physics, DOI: 10.1007/BF01025401.

Pedruzzi R., Baek B.H., Henderson B.H., Aravanis N., Pinto J.A., Araujo I.B., Nascimento E.G.S., Reis Junior N.C., Moreira D.M., Albuquerque T.T.A. (2019). Performance evaluation of a photochemical model using different boundary conditions over the urban and industrialized metropolitan area of Vitoria, Brazil. Environmental Science and Pollution Research, https://doi.org/10.1007/s11356-019-04953-1.

Pinto J.A., Kumar P., Alonso M.F., Andreao W.L., Pedruzzi R., Santos F.S., Moreira D. M., Albuquerque T.T.A. (2020). Traffic data in air quality modeling: a review of key variables, improvements in results, open problems and challenges in current research. Atmospheric Pollution Research, https://doi.org/10.1016/j.apr.2019.11.018.

Pickering, K.E., Thompson, A.M., Wang, Y., Tao, W.K., McNamara, D.P., Kirchhoff, V.W.J.H., Heikes, B.G., Sachse, G.W., Bradshaw, J.D., Gregory, G.L. and Blake, D.R. (1996). Convective transport of biomass burning emissions over Brazil during TRACE A. J. Geophys. Res. 101: 23993–24012.

Pöschl U., von Kuhlmann R., Poisson N., Crutzen P.L. (2000). Development and Intercomparison of Condensed Isoprene Oxidation Mechanisms for Global Atmospheric Modeling. Journal of Atmospheric Chemistry, https://doi.org/10.1023/A:1006391009798.

Rafee S.A.A., Martins L.D., Kawashima A.B., Almeida D.S., Morais M.V.B., Souza R.V.A., Oliveira M.B.L., Souza R.A.F., Medeiros A.S.S., Urbina V., Freitas E.D., Martin S.T., Martins J.A. (2017). Mobile and stationary sources of air pollutants in the amazon rainforest: a numerical study with WRF-Chem model. Atmospheric Chemistry and Physics, https://doi.org/10.5194/acp-2016-1190.

Rafee S. A. A., Kawashima A. B., Morais M. V. B., Urbina V., Martins L. D., Martins J. A. (2015). Assessing the Impact of Using Different Land Cover Classification in Regional Modeling Studies for the Manaus Area, Brazil. Journal of Geoscience and Environment Protection, DOI: 10.4236/gep.2015.36013.

Ring A.M.M., Canty T.P., Anderson D.C., Vinciguerra T.P., He H., Goldberg D.L., Ehrman S.H., Dickerson R.R., Salawitch R.J. (2018). Evaluating commercial marine emissions and their role in air quality policy using observations and the CMAQ model. Atmospheric Environment, https://doi.org/10.1016/j. atmosenv.2017.10.037.

Rozoff C.M., Cotton W.R., Adegoke J.O. (2003). Simulation of St. Louis, Missouri, Land Use Impacts on Thunderstorms. Journal of Applied Meteorology and Climatology, https://doi.org/10.1175/1520-0450(2003)042<0716:SOSLML>2.0.CO;2.

Rosário, N.E., Longo, K.M., Freitas, S.R., Yamasoe, M.A., and Fonseca, R.M. (2013). Modeling the South American regional smoke plume: Aerosol optical depth variability and surface shortwave flux perturbation. Atmos. Chem. Phys. 13: 2923–2938.

Skamarock W. C., Klemp J. B., Dudhia J., Gill D. O., Barker D., Duda M. G., Powers J. G. (2008). A Description of the Advanced Research WRF Version 3 (No. NCAR/TN-475+STR). University Corporation for Atmospheric Research, doi:10.5065/D68S4MVH.

Saldiva P.H.N., Lichtenfels A.J. F. C., Paiva P.S.O., Barone I.A., Martins M.A., Massad E., Pereira J.C.R., Xavier V.P., Singer J.M., Böhm G.M. (1994). Association between air pollution and mortality due to respiratory diseases in children in São Paulo: a preliminary report. Environmental Research, doi.org/10.1006/ENRS.1994.1033.

Seinfeld, J.H. and Pandis, S.N. (2016) Atmospheric Chemistry and Physics: From Air Pollution to Climate Change. John Wiley & Sons, Hoboken.

Silva Dias, M.A.F. (2006). Meteorologia, desmatamento e queimadas na Amazônia: Uma síntese de resultados do LBA. Rev. Bras. Meteorol. 21: 190–199.

Shimada S, Ohsawa T, Chikaoka S, Kozai K (2011) Accuracy of the wind speed profile in the lower PBL as simulated by the WRF model. SOLA 7:109–112. https://doi.org/10.2151/sola.2011-028

Simpson D., Benedictow A., Berge H., Bergström R., Emberson L. D., Fagerli H., Flechard C. R., Hayman G. D., Gauss M., Jonson J. E., Jenkin M. E., Nyíri A., Richter C., Semeena V. S., Tsyro S., Tuovinen J.-P., Valdebenito Á., and Wind P. (2012). The EMEP MSC-W chemical transport model – technical description, Atmospheric Chemistry and Physics, https://doi.org/10.5194/acp-12-7825-2012.

Song S.-K., Shon Z.-H., Kang Y.-H., Kim K.-H., Han S.-B., Kang M., Bang J.-H., Oh I. (2019). Source apportionment of VOCs and their impact on air quality and health in the megacity of Seoul. Environmental Pollution, https://doi.org/10.1016/j. envpol.2019.01.102.

Setzer A., and Pereira M. (1991). Amazonia biomass burnings in 1987 and an estimate of their tropospheric emissions, Ambio, 20, 19 – 22.

Sayer A. M., Hsu N. C., Bettenhausen C., Lee J., Kim W. V., and Smirnov A. (2017). Satellite Ocean Aerosol Retrieval (SOAR) Algorithm Extension to S-NPP VIIRS as Part of the "Deep Blue" Aerosol Project. Journal of Geophysical Research: Atmospheres, doi:10.1002/2017JD027412.

Souto-Oliveira C.E., Andrade M.F., Kumar P., Lopes F.J.S., Babinski M., and Landulfo E. (2016). Effect of vehicular traffic, remote sources and new particle formation on the activation properties of cloud condensation nuclei in the megacity of São Paulo, Brazil. Atmospheric Chemistry and Physics, doi:10.5194/acp-16-14635-2016.

Stockwell W. R., Kirchner F., Kuhn M. and Seefeld S. (1997). A new mechanism for regional atmospheric chemistry modeling, Journal of Geophysical Research, https://doi.org/10.1029/97JD00849.

Stein, O., Schultz, M. G., Bouarar, I., Clark, H., Huijnen, V., Gaudel, A., George, M., and Clerbaux, C.: On the wintertime low bias of Northern Hemisphere carbon monoxide found in global model simulations, Atmos. Chem. Phys., 14, 9295–9316, https://doi.org/10.5194/acp-14-9295-2014, 2014.

Sasano Y. and Nakane H. (1984). Significance of the extinction/backscatter ratio and the boundary value term in the solution for the two-component lidar equation. Applied Optics, https://doi.org/10.1364/AO.23.0011_1, 1984.

Souza, D.Z., Vasconcellos, P.C., Lee, H., Aurela, M., Saarnio, K., Teinila, K., Hillamo, R., € 2014. Composition of PM2.5 and PM10 collected at urban sites in Brazil. Aerosol Air Qual. Res. 14, 168e176. http://dx.doi.org/10.4209/aaqr.2013.03.0071.

Tie X.., Madronich S., Li G.H., Ying Z.M., Zhang R.Y., Garcia A.R., Lee–Taylor J., Liu Y.B. (2007). Characterizations of chemical oxidants in Mexico City: A regional chemical dynamical model (WRF–Chem) study. Atmospheric Environment 41, 1989–2008.

Tewari M., Chen F., Wang W., Dudhia J., LeMone M. A., Mitchell K., Ek M., Gayno G., Wegiel J., and Cuenca R. H. (2004). Implementation and verification of the unified NOAH land surface model in the WRF model. 20th conference on weather analysis and forecasting/16th conference on numerical weather prediction, pp. 11–15.

United Nations, Department of Economic and Social Affairs, Population Division (2018). World Urbanization Prospects: The 2018 Revision. https://population.un.org/wup/Publications/. Accessed, July 13, 2019.

Vasconcellos, P.C., Souza, D.Z., S anchez-Ccoyllo, O., Bustillos, J.O.V., Lee, H., Santos, F.C., Nascimento, K.H., Araújo, M.P., Saarnio, K., Teinila, K., Hillamo, R., € 2010. Determination of anthropogenic and biogenic compounds on atmospheric aerosol collected in urban, biomass burning and forest areas in S~ ao Paulo, Brazil. Sci. Total Environ. 408 (23), 5836e5844. http://dx.doi.org/10.1016/ j.scitotenv.2010.08.012.

Vara-Vela A., Andrade M.F., Kumar P., Ynoue R.Y., Munoz A.G. (2016). Impact of vehicular emissions on the formation of fine particles in the São Paulo metropolitan area: a numerical study with the WRF-Chem model. Atmospheric Chemistry and Physics, https://doi.org/10.5194/acp-16-777-2016, 2016.

Vara-Vela A., Andrade M.F., Zhang Y., Kumar P., Ynoue R.Y., Souto-Oliveira C.E., Lopes F.J.S., Landulfo E. (2018). Modeling of atmospheric aerosol properties in the São Paulo Metropolitan Area: impact of biomass burning. Journal of Geophysical Research, https://doi.org/10.1029/2018JD028768.

Yu M., Zhu Y., Lin C.-J., Wang S., Xing J., Jang C., Huang J., Huang J., Jin J., Yu L. (2019). Effects of air pollution control measures on air quality improvement in Guangzhou, China. Journal of Environmental Management, https://doi.org/10.1016/j. jenvman.2019.05.046.

Wang Z.H., Bai Y.H., Zhang S.Y. (2005). A biogenic volatile organic compounds emission inventory for Yunnan Province. J Environ Sci (China). 2005;17(3):353-359.

Wang K., Zhang Y., Yahya K., Wu S.-Y., & Grell G. (2015). Implementation and initial application of new chemistry-aerosol options in WRF/Chem for simulating secondary organic aerosols and aerosol indirect effects for regional air quality, Atmospheric Environment, https://doi.org/10.1016/j.atmosenv.2014.12.007.

Wang N., Lyu X.P., Deng X.J., Guo H., Deng T., Li Y., Yin C.Q., Li F., Wang S.Q. (2016). Assessment of regional air quality resulting from emission control in the Pearl River Delta region, southern China. Science of the Total Environment, https://doi. org/10.1016/j.scitotenv.2016.09.013.

Wechsler S. Statistics at Square One. 9th ed. London, UK: BMJ Publishing Group.

Zang H, Pu Z, Zang X (2013) Examination of errors in near-surface temperature and Wind from WRF numerical simulations in regions of complex terrain. Weather Forecast 28:893–914. https://doi.org/ 10.1175/WAF-D-12-00109.1

Zhang Y. (2008). Online-coupled meteorology and chemistry models: History, current status, and outlook. Atmospheric Chemistry and Physics, https://doi.org/10.5194/acp-8-2895-2008.

Zhang L., Lin J., Qiu R., Hu X., Zhang H., Chen Q., Tan H., Lin D., Wang J. (2018). Trend analysis and forecast of PM2.5 in Fuzhou, China using the ARIMA model. Ecological Indicators, https://doi.org/10.1016/j.ecolind.2018.08.032.

Declaration of interests

☒ The authors declare that they have no known competing financial interests or personal relationships that could have appeared to influence the work reported in this paper.

☐The authors declare the following financial interests/personal relationships which may be considered as potential competing interests:

Manuscript title:

"Atmospheric aerosols over the state and metropolitan area of São Paulo, Brazil modeled by EURAD-IM on high-resolution: Assessing the influences of remote and local pollutant sources and model performance"

CRediT author statement

Ediclê De Souza Fernandes Duarte: Conceptualization, Methodology, Validation, Formal analysis, Writing, Visualization. **Philipp Franke:** Software, Resources, Writing - Review & Editing, Supervision. **Anne Caroline Lange:** Software, Resources, Writing - Review & Editing, Supervision. **Elmar Friese:** Software, Resources. **Fábio Juliano da Silva Lopes**: Validation, Formal analysis, Resources, Data Curation, Writing - Review & Editing, Visualization. **Jonatan João da Silva**: Data Curation. **Eduardo Landulfo**: Resources., **Cláudio Moises Santos e Silva**: Supervision, **Hendrik Elbern:** Conceptualization, Methodology, Resources, Writing, Supervision, Project administration. **Judith Johanna Hoelzemann:** Conceptualization, Methodology, Validation, Formal analysis, Validation, Resources, Writing, Visualization, Supervision, Project administration.